Intraseasonal and interannual variability of the quasi-two day wave in the Northern Hemisphere summer mesosphere

J. P. McCormack[1], L. Coy[2,3], W. Singer[4]

Corresponding author: J. P. McCormack, Space Science Division, Naval Research Laboratory, 4555 Overlook Avenue SW, Washington DC, 20375, USA. (john.mccormack@nrl.navy.mil)

[1]Space Science Division, Naval Research Laboratory, Washington DC, USA.

[2]Global Modeling and Assimilation Office, NASA Goddard Space Flight Center, Greenbelt MD, USA

[3]Science Systems and Applications Inc., Lanham MD, USA

[4]Leibniz Institute of Atmospheric Physics, Kühlungsborn, Germany

Abstract. This study uses global synoptic meteorological fields from a high-altitude data assimilation system to investigate the spatial and temporal characteristics of the quasi-2 day wave (Q2DW) and migrating diurnal tide during the Northern Hemisphere summers of 2007, 2008, and 2009. By applying a 2-dimensional fast Fourier transform to meridional wind and temperature fields, we are able to identify Q2DW source regions and to diagnose propagation of Q2DW activity into the upper mesosphere and lower thermosphere. We find that Q2DW is comprised primarily of westward propagating zonal wavenumber 3 and wavenumber 4 components that originate from within baroclinically unstable regions along the equatorward flank of the summer midlatitude easterly jet. Amplitude variations of wavenumbers 3 and 4 tend to be anti-correlated throughout the summer, with wavenumber 3 maximizing in July and wavenumber 4 maximizing in late June and early August. Monthly mean Q2DW amplitudes between 30° – 50°N latitude are largest when diurnal tidal amplitudes are smallest and vice versa. However, there is no evidence of any rapid amplification of the Q2DW via nonlinear interaction with the diurnal tide. Instead, variations of Q2DW amplitudes during July are closely linked to variations in the strength and location of the easterly jet core from one summer to the next, with a stronger jet producing larger Q2DW amplitudes. Linear instability model calculations based on the assimilated wind fields find fast growing zonal wavenumber 3 and 4 modes with periods near 2 days in the vicinity of the easterly jet.

1. Introduction

Wind and temperature observations in the MLT over the last several decades show that one of the largest recurring features in MLT dynamics is an eastward-propagating zonal wavenumber 3 disturbance with a period near 48 hours that is commonly referred to as the quasi-two day wave or Q2DW [e.g. Muller and Nelson, 1978; Harris, 1994; Lima et al., 2004; Pancheva, 2006; Hecht et al., 2010; Suresh Babu et al., 2011]. Satellite-based measurements of temperature and long-lived constituents [e.g. Wu et al., 1996; Limpasuvan and Wu, 2003; Garcia et al., 2005; Tunbridge et al., 2011], in combination with satellite-based MLT wind observations [Wu et al., 1993; Lieberman, 1999; Limpasuvan and Wu, 2009], have shown that Q2DW amplitudes peak in the extratropical MLT during both Southern Hemisphere (SH) and Northern Hemisphere (NH) summer shortly after solstice. As an example, Figure 1 plots temperature and meridional wind fields at 40°N and 0.02 hPa ($\sim$ 75 km) during July 2009 showing the longitude-time signature of the eastward propagating Q2DW.

The Q2DW is currently understood to originate primarily from baroclinically unstable regions on the equatorward flank of the summertime mesospheric easterly jet. These regions produce fast-growing instabilities that can project onto the zonal wavenumber 3 global Rossby-gravity mode [Salby, 1981; Plumb, 1983; Pfister, 1985; Lieberman, 1999; Rojas and Norton, 2007]. One key aspect of the Q2DW that is not yet well understood is the cause of its intermittency, i.e., it is often observed in "bursts" throughout the summer season that vary in duration from several days to several weeks (see, e.g., Fig. 1). As a result, the observed Q2DW can exhibit a high degree of both intraseasonal and interannual

variability as documented by Wu et al. [e.g. 1996]; Limpasuvan and Wu [e.g. 2003]; Garcia et al. [e.g. 2005]; Tunbridge et al. [e.g. 2011]; Offerman et al. [e.g. 2011].

Since conditions for baroclinic instability are extremely sensitive to gradients in background zonal wind and temperature, the behavior of the summertime extratropical Q2DW depends on complex interactions with the effects gravity wave drag and solar tides. For example, Norton and Thuburn [1999] used a global circulation model (GCM) to demonstrate that the effects of gravity wave drag maintain the meridional and vertical gradients in the summertime MLT zonal wind distribution that are necessary for the growth of baroclinically unstable local modes. In addition, Salby and Callaghan [2008] showed that the presence of the migrating diurnal solar tide in a primitive equation model effectively can increase the damping of the Q2DW and thus limit its growth under solstice conditions through nonlinear wave-wave interactions. Under certain conditions, nonlinear interactions between the Q2DW and the migrating diurnal tide can also cause a rapid growth in Q2DW amplitude and a contemporaneous (albeit smaller) reduction in the diurnal tidal amplitude. This process was first noted in the observational study by Teitelbaum and Vial [1991], and later described in several modeling studies [Norton and Thuburn, 1999; Palo et al., 1999; Salby and Callaghan, 2008; Chang et al., 2011]. Key factors determining whether or not this rapid amplification of the Q2DW will occur are a strong easterly jet in the summer upper mesosphere and phase locking of the Q2DW with the diurnal cycle (i.e., a 48-hour period) [Walterscheid and Vincent, 1996]. These conditions, and subsequent Q2DW-tide interactions, have been observed in the SH summer MLT [Hecht et al., 2010; McCormack et al., 2010], but it is not clear whether or not such processes also contribute to variability in the Q2DW during NH summer.

The goal of this investigation is to examine the roles of both baroclinic instability mechanisms and possible Q2DW-tidal interactions in controlling Q2DW intermittency in the NH summer extratropical MLT. Doing so requires a data set of global winds and temperatures up to the lower thermosphere (∼90 km) with sufficient temporal resolution to separate the Q2DW and tidal signatures. Presently, such information cannot be obtained from a single set of observations, but can instead be obtained by combining multiple sets of MLT observations using a high-altitude data assimilation system (HDAS). This study examines Q2DW and tidal variability using 6-hourly synoptic meteorological analyses of winds and temperature from the surface to 90 km altitude over the June-August periods of 2007, 2008, and 2009 produced by the Navy Operational Global Atmospheric Prediction System with Advanced Level Physics-High Altitude (NOGAPS-ALPHA). The NOGAPS-ALPHA HDAS has been used previously to describe Q2DW variability in the SH extratropics during January [McCormack et al., 2009], and to provide evidence of nonlinear Q2DW-tidal interactions in the extratropical SH summer MLT region [McCormack et al., 2010]. This is the first study using HDAS fields to examine the behavior of the Q2DW and tides in the NH summer.

Most studies of the Q2DW to date have focused on the SH summer extratropics, where its amplitude is largest. Although the amplitude of the Q2DW in the NH is smaller than its SH counterpart, it has a more complex spatial structure consisting of zonal wavenumbers 2, 3, and 4 whose relative amplitudes vary over the course of the season [Tunbridge et al., 2011]. We employ space-time spectral analysis of the NOGAPS-ALPHA wind and temperature fields to discriminate among the different spatio-temporal components of the Q2DW and the diurnal tide, which is not possible using ground-based data sets or

asynoptic satellite records alone given their limitations in spatial and temporal coverage. This information is used to characterize the seasonal and interannual variability in the NH Q2DW in relation to the migrating diurnal tide. NOGAPS-ALPHA winds are also used as input for a linear instability model to diagnose the origin and growth of the Q2DW throughout the NH summer via baroclinic instability. The results of this investigation indicate that the strength and location of the midlatitude mesospheric easterly jet core is the main factor controlling the behavior of the Q2DW during NH summer.

The NOGAPS-ALPHA HDAS system and data analysis techniques are described in Section 2. Section 3 presents the seasonal and interannual variability in the QW2DW and diurnal migrating tide during NH summer of 2007, 2008, and 2009. Section 4 discusses the origin and propagation of the Q2DW using diagnostic wave activity calculations. Section 5 presents results from a linear instability model that uses NOGAPS-ALPHA assimilated winds to examine how the Q2DW arise from baroclinically unstable regions near the summer easterly jet. Section 6 contains a summary of these results and explores future research directions.

2. Data and Methodology

The NOGAPS-ALPHA HDAS assimilates operational meteorological observations in the troposphere and lower stratosphere in combination with research satellite observations of middle atmospheric temperature, ozone, and water vapor to provide a comprehensive analysis of atmospheric state variables from the surface to ∼90 km. In this section, we first present a brief overview of the HDAS system. For a comprehensive description of the production version of NOGAPS-ALPHA, see Eckermann et al. [2009a]. We then discuss

the methods used to analyze the behavior of the Q2DW and diurnal migrating tide in the NH summer MLT.

2.1. NOGAPS-ALPHA Description

NOGAPS-ALPHA is built upon the framework of the NOGAPS numerical weather prediction and analysis system that originally extended from the surface to 1 hPa (∼50 km). It consists of two main components: a global spectral forecast model [Hogan and Rosmond, 1991], and a three-dimensional variational (3DVAR) data assimilation algorithm [Daley and Barker, 2001]. To expand this system's meteorological analysis capability through the middle atmosphere, the vertical domain of the NOGAPS-ALPHA forecast model was raised to ∼100 km [Hoppel et al., 2008], and a 68-level (L68) hybrid $\sigma - p$ vertical coordinate was introduced [Eckermann, 2009b], giving ∼2 km spacing of levels throughout the stratosphere and mesosphere. In the present study, the forecast model component of NOGAPS-ALPHA uses a T79 horizontal wave number truncation to give an effective horizontal grid spacing of 1.5° in longitude and latitude on a quadratic Gaussian grid. Extending NOGAPS-ALPHA into the middle atmosphere required the addition of several new physics packages, as described in Eckermann et al. [2009a]. These include improved shortwave heating and longwave cooling rates [Chou et al., 2001; Chou and Suarez, 2002], updated paramterizations of sub-grid scale orographic [Palmer et al., 1986] and non-orographic gravity wave drag [Eckermann, 2011], and linearized photochemical parameterizations for middle atmospheric ozone and water vapor [McCormack et al., 2006, 2009], which are both prognostic model variables in NOGAPS-ALPHA.

The data assimilation component of NOGAPS-ALPHA is based on the NRL Atmospheric Variational Data Assimilation System (NAVDAS) [Daley and Barker, 2001], a

3DVAR system with a 6-hour update cycle that assimilates both conventional ground-based observations (e.g., wind, pressure, temperature from station reports and radiosondes) and operational satellite-based observations (e.g., microwave radiances, surface winds, precipitable water). In addition, NOGAPS-ALPHA assimilates Aura MLS Version 2.2 temperature, O_3, and H_2O profile measurements [Hoppel et al., 2008]. The Aura satellite completes ∼13 orbits per day with coverage between 82°S–82°N latitude. NOGAPS-ALPHA also assimilates Version 1.07 temperature profile measurements from the TIMED SABER instrument, which is a side-viewing instrument whose latitude coverage alternates every two months to view high latitudes in both hemispheres. During NH summer, TIMED switches from its north-viewing mode (latitude range of 83°N to 52°N) to south-viewing mode (52°N to 83°S) in mid-July. This change in coverage is not seen to affect the Q2DW in the NOGAPS-ALPHA analyses, whose amplitude generally maximizes between 30°–40°N latitude.

The bulk of the information on the Q2DW and tides in the NOGAPS-ALPHA analyses comes from MLS and SABER temperature profiles that are assimilated between the 32 – 0.002 hPa pressure levels. The vertical resolution of the SABER temperature retrieval remains ∼2 km throughout the stratosphere and mesosphere while the resolution of the MLS temperature retrieval degrades from ∼3 km in the stratosphere to ∼13 km near the 0.01 hPa level. Global mean systematic biases of 2–3 K between the MLS and SABER temperatures, have been removed prior to assimilation to avoid introducing spurious spatial variability into the temperature analyses, as described in the work of Hoppel et al. [2008]. To obtain accurate heating and cooling rates in the middle atmosphere,

158 NOGAPS-ALPHA also assimilates daily MLS H_2O and O_3 profiles between 220–0.002
159 hPa and 215–0.02 hPa, respectively [Eckermann et al., 2009a].

160 To investigate the Q2DW in the NH MLT, the present study analyzes global synoptic
161 zonal and meridional wind fields produced by the NOGAPS-ALPHA HDAS. NOGAPS-
162 ALPHA does not directly assimilate middle atmospheric wind measurements; instead, it
163 uses a formulation of the gradient wind approximation in the off-diagonal elements of
164 the observation error covariance matrix to produce balanced wind and temperature incre-
165 ments. These increments are integrated forward in time by the forecast model component,
166 and the resulting middle atmospheric wind fields are further constrained by the physical
167 parameterizations in the model (e.g., gravity wave drag, diffusion, etc.). As previous
168 studies have shown [McCormack et al., 2009, 2010] the resulting 6-hourly global wind and
169 temperature fields have the spatial and temporal resolutions necessary to discriminate
170 between the Q2DW and diurnal tide in the SH summer MLT; the present study extends
171 these investigations to the NH summer.

172 A critical test of any assimilation system is verification with independent observations.
173 For middle atmospheric winds and temperatures, these types of observations consist
174 mainly of ground-based radar and lidar measurements over a relatively small number
175 of locations. Eckermann et al. [2009a] and Stevens et al. [2010] show that diurnal and
176 semi-diurnal variations in the NOGAPS-ALPHA MLT wind and temperature fields agree
177 well with independent ground-based observations at high northern latitudes during the
178 2007 summer season. McCormack et al. [2010] also showed good agreement between the
179 Q2DW in NOGAPS-ALPHA MLT winds and medium-frequency radar winds during Jan-

uary 2006 and January 2008. Furthermore, NOGAPS-ALPHA winds compared well with Tromsø meteor radar winds at 70°N during January 2009 [Coy et al., 2011].

To demonstrate that NOGAPS-ALPHA MLT winds used in the present study agree with ground-based observations during NH summer, Figure 2 compares meridional winds at 88 km altitude from meteor radar observations over Kühlungsborn (54°N, 12°E) with corresponding NOGAPS-ALPHA winds at 0.0036 hPa during July and August 2007. To facilitate the comparison, a 5-point smoothing was applied to the hourly meteor wind values in order to reduce high-frequency variability. As Fig. 2 shows, there is very good overall agreement between the NOGAPS-ALPHA analyzed winds and the meteor radar winds at this location. In particular, both data sets show clear 2-day periodicity during July (days 196-208). Although additional comparisons are desirable to fully verify the NOGAPS-ALPHA analyses, results to date clearly demonstrate that the analyzed winds can capture key features of the Q2DW.

2.2. Space-Time Spectral Analysis

To describe the characteristics of the Q2DW and diurnal migrating tide, we use a two-dimensional fast Fourier transform (2DFFT) approach following Hiyashi [1971], where NOGAPS-ALPHA wind and temperature fields at a given latitude and pressure level are expanded as Fourier series in longitude and time. Following the procedure described in McCormack et al. [2009], daily zonal means are subtracted from each 6-hourly longitude-time field and then a cosine taper is applied to the first and last 10% of each record in time. The resulting space-time power spectrum describes the amount of variance at each frequency and zonal wave number. The 2DFFT is applied over a 32-day interval to derive

results for an individual month. It is also applied over a 90-day interval to obtain results over the summer period June-August.

Figure 3 plots the resulting normalized power spectrum derived for a 32-day period (128 points) of 6-hourly NOGAPS-ALPHA meridional winds from 30 June – 31 July 2009 at 0.02 hPa and 40°N (see Fig. 1b). The 2DFFT method can identify both westward and eastward propagating features that are associated, by convention, with positive and negative frequency values respectively. At this particular level, only westward features are found and so only positive frequencies are plotted.

The results of the 2DFFT in Fig. 3 show that most of the variance in the meridional winds at this location is found in westward–propagating zonal wavenumbers 3 and 4 with frequencies between 0.45–0.6 cpd. Similar results are found in the 2DFFT analysis of NOGAPS-ALPHA temperature at this location (not shown). This combination of waves 3 and 4 at periods near 2 days is consistent with the recent study of MLS temperatures by Tunbridge et al. [2011], who found the Q2DW throughout the NH summer MLT to be a complex of waves 2, 3, and 4. Fig. 3 also indicates variance at wave 1 centered on 1 cpd, indicative of the migrating diurnal tide. It should be noted that although spectral analysis of the 6-hourly NOGAPS-ALPHA output can resolve frequencies down to 2 cpd, the 3DVAR system's ±3-hour assimilation window may not be able to fully capture this high-frequency variability associated with, e.g., the semi-diurnal tide. Therefore, this study focuses on interactions between the Q2DW and diurnal tide.

To study the episodic nature of the Q2DW-tide interactions throughout the NH summer season, time series of the individual Q2DW and tide components in the wind and temperature fields are reconstructed by applying appropriate band-pass filters to the in-

verse 2DFFT. Based on the results of the power spectra in Fig. 3, pass bands at zonal wavenumbers 3 and 4 from 0.45–06 cpd are chosen for the Q2DW, and at zonal wave 1 from 0.9–1.1 cpd for the diurnal tide. Eddy heat and momentum fluxes calculated from these filtered fields are then used to formulate Eliassen-Palm (EP) flux diagnostics of wave activity associated with the Q2DW [Lieberman, 1999]. This technique has been applied previously to NOGAPS-ALPHA fields to investigate the evolution of the Q2DW and diurnal tide in the SH summer mesosphere [McCormack et al., 2009, 2010]. In the present study, we extend this analysis to focus on the behavior of the Q2DW and diurnal migrating tide during the NH summers of 2007, 2008, and 2009.

3. 2DFFT Results

This section presents detailed information on the latitude and altitude structure of the Q2DW and migrating diurnal tide during NH summer obtained from the 2DFFT analysis of the NOGAPS-ALPHA temperature and meridional wind fields. This section also discusses both the interannual and intraseasonal variability of these features during June-August of 2007, 2008, and 2009.

3.1. Interannual variability of the Q2DW

Figure 4 plots monthly mean values of the root-mean-square amplitude for the westward propagating zonal wavenumber 3 component of the Q2DW in both temperature and meridional wind (referred to in terms of its central frequency and wavenumber as [0.5,3]) for July 2007, 2008, and 2009. In all three years, the spatial structure of the Q2DW is consistent with earlier observations of the NH summer [e.g. Tunbridge et al., 2011, their Figure 7]. Specifically, we find that the feature exhibits deep vertical extent throughout

the mesosphere between 20°N–55°N with a maximum in temperature near 40°N and 0.02 hPa (∼75 km). Fig. 4 also shows that the peak monthly mean temperature amplitudes vary from year to year, reaching 3.1 K in 2007, 3.8 K in 2008, and 4.5 K in 2009. A secondary maximum in [0.5,3] amplitude is noted in all three years between 50°N–60°N above 0.001 hPa (∼96 km), reaching 2.9K, 4.9K, and 4.0K in 2007, 2008, and 2009 respectively. While this secondary temperature maximum appears to be related to the [0.5,3] meridional wind component near 95 km, it should be regarded with some caution as it lies above the top pressure level of 0.002 hPa where MLS and SABER temperature observations are assimilated.

The interannual variability in monthly mean meridional wind [0.5,3] amplitudes shown in Fig. 4 matches that of the monthly mean temperature amplitudes. Specifically, for the three years analyzed the Q2DW in meridional wind is strongest in July 2009 (peak value of 19 m s^{-1}) and weakest in July 2007 (peak value of 15 m s^{-1}). The spatial structure of the meridional wind [0.5,3] component is also consistent from year to year, and exhibits three key features: (1) A broader latitude range compared to the temperature Q2DW, extending from the summer hemisphere across the equator to 20°S; (2) a maximum near 95 km between 40°N– 50°N; and (3) a pronounced poleward tilt with increasing height. These features are in good qualitative agreement with model simulations of the [0.5,3] feature in meridional wind [Norton and Thuburn, 1999; Palo et al., 1999; Salby and Callaghan, 2000; Chang et al., 2011].

Figure 5 plots the monthly mean amplitudes of the [0.5,4] component in NOGAPS-ALPHA temperatures and meridional winds. While the latitude and altitude dependences of the [0.5,4] temperature component are similar to the [0.5,3] component, we find that

the peak values of [0.5,4] in temperature are located on average ∼5° equatorward and ∼10–12 km lower than the location of the [0.5,3] temperature peaks. Peak values of the [0.5,4] meridional wind response are also shifted equatorward by ∼5°, on average, relative to the peak [0.5,3] wind values. One main difference between the zonal wave number 3 and 4 features, however, is that the [0.5,4] meridional wind amplitudes do not exhibit the sharp increase with height seen in the [0.5,3] wind amplitudes. Another important difference is that, on average, both the peak temperature and wind amplitudes of [0.5,4] are 30% less than the amplitudes of [0.5,3].

We note here that Tunbridge et al. [2011] found evidence for a westward zonal wave number 2 feature associated with the Q2DW in NH summer based on analysis of MLS temperatures. Our 2DFFT analysis of NOGAPS-ALPHA temperatures finds that peak amplitudes for this [0.5,2] component are typically less than 1.5 K and, unlike the zonal wave 3 and 4 cases, are found over a broad latitude region from 10°N–70°N above ∼80km. The latitude and altitude dependences of the [0.5,2] component in meridional wind (not shown) are also markedly different from the zonal wave number 3 and 4 cases, showing peak values of ∼10 m s^{-1} throughout the upper mesosphere centered over the equator. Because this apparent wave number 2 Q2DW exhibits spatial characteristics that are fundamentally different from [0.5,3] and [0.5,4] results, the present study will focus on the dynamical factors controlling the growth and evolution of wave number 3 and 4 components of the Q2DW in NH summer. Possible relationships between these components and the zonal wave number 2 Q2DW will be examined in a future study.

One distinct advantage of 6-hourly global HDAS output is the ability to discriminate among the diurnal migrating (or [1,1]) tide and the [0.5,3] and [0.5,4] components of

290 the Q2DW. As discussed in the Introduction, there is both theoretical and observational
291 evidence that the Q2DW can be influenced by tides, and vice versa. Most of these studies,
292 however, focus on the SH summer period when Q2DW amplitudes are larger than during
293 NH summer. We next examine the general characteristics of the [1,1] tide obtained from
294 the 2DFFT analysis for June–August of 2007, 2008, and 2009.

295 Figure 6 plots the monthly mean [1,1] amplitudes in both temperature and meridional
296 wind for July 2007, 2008, and 2009. The latitude and altitude structure of the tidal
297 amplitudes derived from NOGAPS-ALPHA fields are quite similar from year to year, and
298 are in good agreement with earlier modeling studies [e.g. Norton and Thuburn, 1999;
299 Chang et al., 2011]. Of the three summers studied here, we find that mean July tidal
300 amplitudes in temperature and meridional wind are generally smallest in 2009. The
301 spatial structure of the [1,1] meridional wind amplitudes (Figs. 6b, 6d, and 6f) in the
302 region between 30°N–40°N, where Q2DW amplitudes are largest, exhibits a pronounced
303 vertical gradient during both July 2008 and July 2009. This gradient produces a very sharp
304 "cutoff" in the tidal response below the 0.003 hPa level (∼90 km) in these two years. In
305 contrast, the tidal response in July 2007 between 30°N–40°N has a much weaker vertical
306 gradient, and there is no corresponding cutoff in tidal amplitudes below 0.003 hPa. As a
307 result, the [1,1] meridional wind amplitudes between 30°N–40°N in the 85–90 km region
308 are relatively large (∼20 m s^{-1}) during July 2007. During July 2007 and 2008, on the other
309 hand, the [1,1] meridional wind amplitudes in this region range from 8–12 m s^{-1}. Overall,
310 the smallest July Q2DW amplitudes in the Northern subtropical upper mesosphere were
311 found in 2007, when the corresponding monthly mean tidal amplitudes were largest. This

anti-correlation of the Q2DW and tidal amplitudes is generally consistent with previous studies, and will be examined further in the following section.

The interannual variations in tidal amplitudes seen in Fig. 6 can be caused by a variety of different factors, including variations in the strength of tidal forcing (i.e., latent heat release and ozone heating), and variations in the strength of the zonal winds in MLT. The latter is highly dependent on gravity wave drag, and wind variations in the stratosphere can act as a filter for upward propagating gravity waves. An analysis of TIMED Doppler Interferometer winds from 2002–2007 by Wu et al. [2008] found that amplitudes of the migrating diurnal tide tend to be larger during the westerly phase of the stratospheric quasi-biennial oscillation (QBO). We note that the QBO was in its easterly phase during July 2007; during July 2008 and 2009, winds in the equatorial lower stratosphere were westerly. Therefore, it does not appear that the QBO can explain the interannual variations in the Northern subtropical tidal amplitudes shown in Figure 6. Regardless of the origin, the results in Figs. 6 and 7 are consistent with the interpretation that strong tidal amplitudes can limit the growth of the Q2DW, as discussed in the Introduction. We examine the relationship between the Q2DW and migrating diurnal tide in more detail in Section 3.3.

3.2. Intraseasonal variability

We next examine the variability of the [0.5,3] and [0.5,4] components over the course of each summer period (June–August). This is done by applying a band-pass filter at zonal wavenumber 3 and 4 with limits of 0.45 – 0.6 cpd to the inverse 2D Fourier transform of the NOGAPS-ALPHA fields over a 75-day interval from June 5 to August 20 of each year. To facilitate comparisons with seasonal Q2DW variability seen in the SH winter reported

by McCormack et al. [2010] , we will focus on the seasonal evolution of the Q2DW seen in NOGAPS-ALPHA meridional wind fields. We note that the time behavior of the Q2DW in temperature during NH summer (not shown) closely matches the time behavior in meridional wind.

Figure 7 plots [0.5,3] amplitudes in meridional wind at 0.021 hPa ($\sim$ 75 km) as a function of latitude and time throughout the NH summers of 2007, 2008, and 2009. In all three cases, the amplitudes exhibit a double-peaked structure during July that can extend from $\sim$50°N across the equator to 20°S. Maximum amplitudes of 17 m s^{-1}, 22 m s^{-1}, and 23 m s^{-1} are found between 30° – 50°N during July of 2007, 2008, and 2009, respectively. The smaller maximum wind amplitude at this level in 2007 is consistent with the smaller monthly mean [0.5,3] amplitudes noted in both temperature and meridional wind throughout the Northern extratropical mesosphere during July 2007 (Fig. 4a,b). We note that the region of peak [0.5,3] amplitude is more narrowly confined in latitude during the 2007 summer case than during the 2008 and 2009 cases.

Figure 8 plots the [0.5,4] meridional wind amplitude at 0.021 hPa for the NH summers of 2007, 2008, and 2009. We find that the seasonal behavior of the wavenumber 4 Q2DW differs considerably from the behavior of wavenumber 3. For example, maximum [0.5,4] wind amplitudes of 22 m s^{-1} and 19 m s^{-1} are found in early August of 2007 and 2009, respectively. In contrast, in 2008 the maximum amplitude of 16 m s^{-1} occurs in late June. Overall, the meridional extent of the [0.5,4] component for all three summers at this level is narrower in latitude than for [0.5,3].

The double-peak structure in the Q2DW amplitudes throughout NH summer are consistent with the results in Tunbridge et al. [2011, their Fig. 10]. This is to be expected,

since the NOGAPS-ALPHA assimilates the same MLS temperature observations (in addition to SABER temperature observations). Offerman et al. [2011] found similar seasonal behavior of the Q2DW from upper mesospheric OH temperature measurements during 2004-2009, i.e., two peaks in Q2DW amplitude in early and late NH summer, although this study was not able to distinguish among different wavenumber components of the Q2DW. Offerman et al. [2011] also reported a peak in Q2DW temperature amplitudes in April, giving rise to an apparent triple-peak structure throughout the NH spring-summer period. We do not, however, find any evidence for Q2DW activity during April or May of 2007, 2008, or 2009 in the present analysis of NOGAPS-ALPHA wind and temperature fields. One possible explanation for this discrepancy may be that the daily sampling rate of the OH temperatures may result in aliasing of tidal variations that produces a a spurious Q2DW signal under equinoctial conditions. Additional direct comparisons between NOGAPS-ALPHA fields and independent observations are needed to further investigate this issue.

3.3. Q2DW - Tide Relationships

Earlier observational studies [Harris, 1994; Lima et al., 2004; Pancheva, 2006; Hecht et al., 2010; McCormack et al., 2010] found correlations between the Q2DW and diurnal migrating tide in meridional winds during SH summer, suggesting nonlinear interactions through which the former grows at the expense of the latter. To determine if there is a relationship between the intraseasonal behavior of the Q2DW and the migrating diurnal tide during NH summer, we next examine the temporal variability of the [1,1] component. Figure 9 plots the [1,1] meridional wind amplitude as a function of latitude and time at 0.0036 hPa (∼88 km) for the NH summer period of 2007, 2008, and 2009. This level is of

particular interest as it lies near the location of peak amplitude in the [0.5,3] component of the meridional winds (see Fig. 4).

The [1,1] signal in NOGAPS-ALPHA meridional wind at 0.0036 hPa is largely confined to the subtropical regions of each hemisphere, which is consistent with earlier studies [e.g. Norton and Thuburn, 1999; Wu et al., 2008; Lieberman, 1999; Chang et al., 2011]. In all three years, the tidal amplitudes are at a minimum near solstice and tend to increase as the summer progresses. A comparison of Figures 7 and 9 indicate an inverse relationship between the amplitudes of the [0.5,3] Q2DW and the diurnal migrating tide that is consistent with earlier observational studies [e.g. Lima et al., 2004; Pancheva, 2006; Hecht et al., 2010]. Specifically, the [1,1] amplitudes are largest in July 2007 when Q2DW amplitudes are smallest. Salby and Callaghan [2008] demonstrated that larger diurnal tidal amplitudes can locally reinforce the Q2DW, which promotes instability and wave breaking that effectively limit the amplification of the Q2DW. GCM studies [e.g Norton and Thuburn, 1999; Palo et al., 1999; Chang et al., 2011] have also shown that when Q2DW amplitudes are large, nonlinear interactions can take place between the [0.5,3] and [1,1] "parent" waves that produce "child" waves whose frequency/wavenumber characteristics are determined from combinations of the sums and differences of the parent waves. In this scenario, the cascade of energy to smaller scales causes the amplitude of the child waves to grow at the expense of the diurnal tide, producing a strong anti-correlation between the the Q2DW and diurnal tide shortly after summer solstice.

To examine the relationships between the Q2DW and diurnal migrating tide in the NH summer, Figure 10 plots time series of the [0.5,3], [0.5,4], and [1,1] amplitudes derived from the 2DFFT analysis at 30°N and 0.0036 hPa over the summers of 2007, 2008, and

2009. Correlation coefficients computed among these time series are listed in Table 1. While there appears to be an inverse relationship between the monthly mean amplitudes of the diurnal migrating tide and the Q2DW from one summer to the next, there is no evidence of a strong anti-correlation between [1,1] and either [0.5,3] or [0.5,4] throughout the month of July to indicate that the Q2DW is growing at the expense of the diurnal migrating tide via nonlinear wave-wave interaction. Of the three months, only July 2008 exhibits a negative correlation between the tide and the Q2DW, and this appears largely to be due to steady declines in the Q2DW amplitudes that are coincident with a steady increase in tidal amplitude. Instead, the highest negative correlations during July 2007 and 2009 are found between [0.5,3] and [0.5,4], suggesting that in some circumstances one component of the Q2DW may be growing preferentially over another. Overall, the lack of a strong anti-correlation between the Q2DW and tide indicates that year-to-year variability in the background state of the NH summertime mesosphere, rather than amplification of the Q2DW due to interaction with the tides, could be responsible for the interannual differences in the amplitudes of the Q2DW seen in Figs. 4 and 5. Possible explanations for this behavior will be explored section 5.

In summary, the results of the 2DFFT analysis find that the Q2DW in the NH summers of 2007, 2008, and 2009 is comprised primarily of zonal wavenumber 3 and wavenumber 4 components whose latitude and altitude structures are consistent with previous observational studies. Monthly mean amplitudes of both [0.5,3] and [0.5,4] components are largest during July 2009, and smallest during July 2007. In all 3 summers, the [0.5,3] component exhibits two periods of peak amplitude; once in early July and again 2-3 weeks later. The [0.5,4] component, on the other hand, tends to exhibit peak amplitudes in late June

425 and early August. To further investigate the origin of the interannual and intraseasonal
426 variability in the Q2DW during these NH summers, the following section examines condi-
427 tions favoring Q2DW growth via baroclinic instability using NOGAPS-ALPHA wind and
428 temperature fields.

4. EP-Flux Diagnostics

429 In this section, we employ a series of diagnostic calculations to examine the origin
430 and growth of the Q2DW in the NH summer based on linear quasigeostrophic theory.
431 Such an approach has been used previously to study the behavior of the Q2DW near
432 the stratopause [Randel, 1994; Orsolini et al., 1997; Limpasuvan et al., 2000] to identify
433 regions of baroclinic and/or barotropic instability favoring Q2DW growth and propagation
434 using daily stratospheric meteorological fields. In the present work, we extend this type
435 of analysis into the upper mesosphere using global synoptic NOGAPS-ALPHA wind and
436 temperature fields.

437 A necessary condition for the growth of the Q2DW in the summer extratropical meso-
438 sphere via baroclinic instability is a reversal of the meridional gradient in quasigeostrophic
439 potential vorticity q [see,e.g. Plumb, 1983; Pfister, 1985]. In spherical coordinates this is
440 computed from the relation

441 $$\overline{q}_{\phi} = \frac{2\Omega}{a} cos\phi - \frac{1}{a}\frac{\partial}{\partial\phi}\left[\frac{1}{acos\phi}\frac{\partial(\overline{u}cos\phi)}{\partial\phi}\right] - (2\Omega sin\phi)^2 e^{z/H}\frac{\partial}{\partial z}\left[\frac{1}{N^2}e^{-z/2H}\frac{\partial\overline{u}}{\partial z}\right] \quad (1)$$

442 where p is pressure in hPa, ϕ is latitude, $\overline{u}$ is the zonal mean zonal wind speed in m s^{-1},
443 H is the scale height, z is the log-pressure vertical coordinate, N is the Brundt-Vaisala
444 frequency, a is the Earth's radius, and Ω is the planetary rotation rate. As equation (1)
445 shows, reversals in $\overline{q}_{\phi}$ (i.e., from positive to negative values) are determined by the curva-

ture in the background zonal wind distribution. Consequently, accurate wind analyses are needed to diagnose baroclinic instability. Here we use global NOGAPS-ALPHA horizontal wind and temperature fields on constant pressure surfaces to compute q_ϕ during July of 2007, 2008, and 2009. This information shows how variations in baroclinic instability from one NH summer to the next may help to explain the observed interannual variations in July Q2DW amplitudes shown in Figs. 4 and 5. While reversal of $\overline{q}_\phi$ is a necessary condition for Q2DW growth through baroclinic instability, it is not sufficient. Conditions must support the growth of the disturbance in the absence of a critical line, i.e., where the speed of the background flow matches the phase speed of the disturbance.

Theory states that growth of the Q2DW is related EP flux divergence in baroclinically unstable regions [e.g. Plumb, 1983]. The EP flux vector can be computed from the eddy heat and momentum fluxes associated with the Q2DW using the relation [see, e.g. McCormack et al., 2009, equation 4]

$$\mathbf{F_p}\,[\phi, z] = \rho a cos\phi \left[-\overline{< u'v' >}\ ,\ (f - \frac{1}{acos\phi}[\bar{u}\ cos\phi]_\phi)\frac{R}{HN^2}\overline{< v'T' >}) \right]. \qquad (2)$$

The terms $\overline{< u'v' >}$, and $\overline{< v'T' >}$ represent zonal mean eddy momentum and heat fluxes, primes denote deviations from the zonal mean and brackets denote a daily average. These quantities are computed from gridded six-hourly NOGAPS-ALPHA zonal wind, meridional wind, and temperature fields that have been band-pass filtered in order to isolate the [0.5,3] or [0.5,4] components of the Q2DW, as described in Section 2.

Calculating EP flux from eddy heat and momentum fluxes related to the Q2DW requires synoptic horizontal wind and temperature fields throughout the MLT region. Although numerous modeling studies have examined EP flux-based diagnostics of the Q2DW, only a few studies have used observations to calculate EP fluxes associated with the Q2DW.

For example, Lieberman [1999] used High Resolution Doppler Imager (HRDI) wind and temperature observations from January 1994 to compute EP flux divergences in the SH summer mesosphere. More recently, the study by Offerman et al. [2011] used geostrophic winds derived from Microwave Limb Sounder (MLS) temperature measurements to relate the occurrence of baroclinically unstable conditions to the seasonal variability in the Q2DW observed from ground-based stations in northern Europe. Here we use output from the NOGAPS-ALPHA global HDAS to describe EP flux divergence associated with both [0.5,3] and [0.5,4] components of the Q2DW in the NH summer.

Figure 11 plots EP flux vectors related to the [0.5,3] Q2DW for three cases: 20 July 2007 (Fig. 10a), 16 July 2008, and 23 July 2009 (Fig. 10c). These three cases were chosen based on the large Q2DW amplitudes observed on these dates (see Fig. 7). Also plotted in Fig. 11 is the daily average zonal mean zonal wind distribution for these days, from which we calculate values of $\overline{q}_{\phi}$. To illustrate the relationship between baroclinically unstable regions and Q2DW growth, shaded regions in Fig. 11 indicate where $\overline{q}_{\phi}$ is negative. In all three cases, Fig. 9 shows EP flux divergence related to the [0.5,3] component of the Q2DW near the core of the easterly jet between 0.05 – 0.1 hPa. The direction of the EP flux vectors indicate propagation of wave activity away from the approximate location of the critical line for the [0.5,3] wave, which is indicated by the bold red contour. In the lower mesosphere the propagation is primarily equatorward, while in the upper mesosphere it is primarily poleward and upward.

Figure 12 plots the EP fluxes of the Q2DW for three cases where amplitudes of the [0.5,4] component were largest during the three NH summers: 4 August 2007 (Fig. 12a), 22 June 2008 (Fig. 12b), and 4 July 2009 (Fig. 12c). Wave activity associated with the

[0.5,4] component originates just equatorward of the easterly jet core between 0.1 – 0.2 hPa and propagates away from the estimated location of the critical line (blue contour in Fig. 12), mainly in the upward and poleward direction. It is interesting to note how the locations of the critical lines in Figs. 11 and 12, which are determined by the curvature of the zonal mean zonal wind, can affect the upward propagation of the Q2DW. For example, in the 2007 case (Fig. 11a) the summer easterly jet is weaker and exhibits a poleward tilt with increasing altitude between 40°–65°N, which leads to a gradual sloping of the critical lines upward and poleward, away from the source regions. In the 2008 and 2009 cases, the jet is stronger and its core is centered between between 40°–50°N, producing a "bull-nose" shape in the location of the critical lines where the equatorward edge of the critical lines extend higher in altitude than in the 2007 case. In particular, the higher extent of the critical lines in the 2009 case (see Fig. 11c and Fig. 12c) appears to direct more Q2DW activity upward into the region above the 0.01 hPa level.

To further examine the relationship between the location of the Q2DW critical line and vertical wave propagation during NH summer, Figure 13 plots the time evolution of zonal mean zonal winds over the NH extratropics during July of 2007, 2008, and 2009 at 0.021 hPa. Superimposed upon the wind contours are regions where q_ϕ is negative (gray shading). Also plotted in Fig. 12 are values of the eddy heat flux (heavy black contours), that are proportional to the vertical component of the EP-flux (equation 2). During July 2007 (Fig. 13a) the location of the [0.5,3] critical line retreats poleward as the month progresses due to the weakening easterly jet. In contrast, the stronger easterly jet during July 2008 and 2009 (Fig. 13b and 13c) maintains the position of the [0.5,3] critical line

514 near 40°N throughout the month. As a result, there are more sustained periods of high
515 eddy heat flux during July 2008 and 2009.

516 These results indicate that the larger monthly mean Q2DW amplitudes in July during
517 2008 and 2009 as compared to July 2007 can be attributed to the characteristics of the
518 summer easterly jet. Specifically, a stronger and more sustained jet core near the Q2DW
519 source region acts to focus more wave activity upward through a smaller area by nature of
520 the critical line's location. A weaker jet core, on the other hand, results in the critical line
521 sloping away from the source region that allows upward wave activity to spread throughout
522 a much wider area. Figure 14 summarizes this relationship, plotting time series of the
523 zonal mean zonal winds at 40°N and 0.1 hPa from 1 June to 31 August of 2007, 2008, and
524 2009. The zonal mean easterly flow was strongest throughout the summer of 2009, when
525 Q2DW amplitudes were largest. During summer 2007, when Q2DW amplitudes were
526 smallest, the easterly jet briefly peaks in early July and is relatively weak both before and
527 after that time. In 2008, the peak winds were somewhat weaker than in 2007, but they
528 were more sustained, coincident with monthly mean Q2DW amplitudes that were larger
529 than 2007.

530 The EP-flux diagnostics based on the NOGAPS-ALPHA meteorological fields indicate
531 that the Q2DW originates from baroclinic instabilities near the equatorward flank of the
532 mesospheric summer easterly jet. The interannual variability of the Q2DW amplitudes
533 in NH summer over the 2007 – 2009 period closely follows interannual variability in the
534 strength and position of the summer easterly jet core, which determines the locations of
535 the critical lines for the [0.5,3] and [0.5,4] components of the Q2DW. As the results in
536 section 3 show, both wavenumber 3 and wavenumber 4 components of the Q2DW are of

comparable magnitude in NH summer, and they both exhibit a high degree of variability throughout the summer season. In the next section, we use a linearized instability model to examine this intraseasonal variability in more detail

5. Instability Model Results

The results in the preceding sections show that both wavenumber 3 and wavenumber 4 components of the Q2DW arise from baroclinically unstable regions near the summer easterly jet at midlatitudes in the the NH mesosphere. As Figures 7 and 8 illustrate, amplitudes of the [0.5,3] component are typically largest in July, while the largest amplitudes of the [0.5,4] component generally occur in late June or early August. This variability is consistent with an earlier study of the NH Q2DW by Tunbridge et al. [2011], which showed that in some years the amplitude of the [0.5,4] component surpasses the amplitude of the [0.5,3] component in August.

To better understand the origins of this behavior, we use a simple linear instability model to examine the characteristics of the fastest-growing unstable modes in the MLT region near the NH summer easterly jet. This approach has been used to study other types of free traveling planetary waves in the MLT [e.g. Hartmann, 1983; Manney and Randel, 1993]. The model is based on the linearized quasi-geostrophic potential vorticity equation for frictionless, adiabatic flow on a β–plane centered at midlatitudes [see, e.g. Andrews et al., 1987, their equation 3.4.5]:

$$q'_t + \overline{u}q'_x + v'\overline{q}_y = 0. \tag{3}$$

Here the potential vorticity is derived from the NOGAPS-ALPHA horizontal wind fields. Formulating the zonal wind and potential vorticity distributions in terms of the

geostrophic stream function and assuming periodic solutions as functions of both latitude and time allows equation (3) to be cast as an eigenvalue problem of the form

$$\mathbf{A}x = c\mathbf{B}x \tag{4}$$

where x is the state vector represented by gridded values of the streamfunction and the complex phase speed c is the eigenvalue. The operator $\mathbf{A}$ is determined from $\overline{u}$ and $\overline{q}_y$, the operator $\mathbf{B}$ is determined from the finite-differenced potential vorticity equation; both $\mathbf{A}$ and $\mathbf{B}$ depend on the zonal wavenumber.

To simplify the calculation, the daily averaged values of NOGAPS-ALPHA zonal wind fields are subsampled onto the instability model domain, which consists of a uniform grid with 20 points in latitude extending from 20° – 60° N latitude and 26 points in altitude extending from 65 – 90 km. For a given day, $\mathbf{A}$ and $\mathbf{B}$ are constructed from using the geostrophic streamfunction and potential vorticity using these subsampled daily averaged zonal winds. Standard numerical codes are then used to solve the eigenvalue problem and obtain $\mathbf{x}$ (i.e., the wave modes) and $\mathbf{c}$ (i.e., phase speeds) for zonal wavenumbers 1 through 6. The fastest growing modes are evaluated in terms of their e-folding times, which are determined from the inverse of the imaginary component of the phase speed for each zonal wavenumber. The periods of the unstable modes are determined from the real component of the phase speed (positive values indicate westward propagation). In addition, each mode's spatial structure contains wind and temperature information from which EP fluxes can be computed.

In this discussion, we focus on the summer of 2009 when the Q2DW was most prominent. We first examine model output for two individual cases: 10 July and 5 August. These

cases were chose to highlight the development of the [0.5,3] and [0.5,4] components of the Q2DW, respectively, during the NH summer of 2009. Figure 15a plots the zonal wind and $\overline{q}_y$ distributions over the model domain for the 10 July case. We find that zonal wavenumbers 3, 4, and 5 exhibit the fastest growth rates, with e-folding times of ∼8–9 days (Fig. 15b). The normalized streamfunction amplitudes of waves 1–4 (Fig. 15c-e) have maxima in the region between 30° – 40°N and 60–70km, which closely resembles the observed spatial structure of the [0.5,3] temperature Q2DW in Figure 4. In general, the period of the fastest growing modes decreases with increasing horizontal scale. On this particular day, the zonal wavenumber 3 (Fig. 14e) solution has a period of 2 days, and the wavenumber 4 solution has a period of 1.5 days.

Figure 16 plots instability model results for the 5 August 2009 case. We find that the fastest growing modes are again at zonal wavenumbers 3, 4, and 5 (Fig. 16b). However, the e-folding times of 3–4 days are much shorter than the July case. The spatial structure of the waves in this case now exhibits two maxima (Figs. 16c-e) centered near 35°N and 45°N. For this August case, the zonal wavenumber 3 (Fig. 16e) solution has a period of 3.1 days and the wavenumber 4 solution has a period of 2.3 days.

In order to determine the direction of wave propagation for the instability model solutions related to the Q2DW, Figure 17 plots EP fluxes calculated from the streamfunctions of the zonal wavenumber 3 and 4 eigenvectors for the July and August cases, respectively. For both cases, the EP-flux vectors derived from the model solutions indicate that most of the upward-propagating wave activity originates near the intersection of the critical line for the Q2DW (blue contour) and the region where $\overline{q}_y$ is negative (enclosed by the red contour). This result is consistent with the EP-flux vectors derived directly from the

603 assimilated winds and temperatures plotted in Figs. 11 and 12, and lends support to the
604 idea that the variability of the NH Q2DW is closely linked to the characteristics of the
605 summer midlatitude easterly jet.

606 The results from these two cases show that the growth time of the Q2DW decreased
607 by a factor of 2–3 between early July and early August 2009. To determine if this is a
608 systematic effect, the stability model was applied to daily average NOGAPS-ALPHA zonal
609 wind throughout the period from 5 June–10 August 2009. Figure 18 plots the resulting
610 values of the period and growth time for both wavenumber 3 and 4 solutions. For plotting
611 purposes, these time series have been smoothed using a 3-point running average. During
612 much of June and early July, both wavenumbers have periods near 2 days (Fig. 18a).
613 Starting in mid-July, the periods increase sharply and then vary in the 3–7 day range
614 thereafter. By late summer, the period of wavenumber 4 is consistently 1-2 days shorter
615 than wavenumber 4. The growth time of wavenumber 4 is shorter than wavenumber 4
616 throughout most of the summer (Fig. 18b), and the growth times of wavenumbers 3 and
617 4 both decrease sharply during late-July and early August. These calculations have also
618 been performed for the summers of 2007 and 2008, and similar decreases in growth times
619 from July to August were found in each case (not shown).

620 As previous studies have shown, the results from these types of model calculations can be
621 highly sensitive to the curvature of the zonal wind fields, and thus averaging or smoothing
622 of the input dynamical fields can affect the results. We present these calculations to
623 better understand, in a qualitative sense, possible factors that contribute to the observed
624 intraseasonal variability of the NH Q2DW. From these results, we can conclude that the
625 baroclinically unstable region along the equatorward flank of the NH summer easterly jet

produces the fastest-growing modes at wavenumbers 3, 4, and 5. During June and July, the periods of the wavenumber 3 and 4 modes most closely match the 2-day period of the Rossby normal mode, and these grow preferentially over other modes.

These results alone do not explain why the observed [0.5,3] component of the Q2DW is larger during July while the [0.5,4] component is larger in June and August. Nor do they account for the sporadic behavior of the Q2DW which tends to produce the double peaked structure observed in, e.g., Figure 7. However, based on the observational and model results presented here, we speculate that one possible explanation for this behavior may be that the faster-growing wavenumber 4 unstable mode tends to emerge initially in June, only to be overtaken by the slower-growing wavenumber 3 mode. The observed anti-correlation between the [0.5,3] and [0.5,4] components of the Q2DW during July 2009 suggests that wavenumber 3 may in fact grow at the expense of wavenumber 4 through some nonlinear interaction. When the Q2DW amplitudes and associated EP fluxes grow large enough to become unstable and dissipate, they modify the vertical shear structure in the background zonal wind such that it no longer produces fast-growing unstable modes at zonal wavenumbers 3 and 4 with periods near 2 days. This would be consistent with the sudden increase in the period of the unstable wave 3 and wave 4 modes in mid-July 2009 (Fig. 18a). As baroclinically unstable regions near the easterly jet reform after the Q2DW dissipates, another fast-growing zonal wave 4 mode can emerge in late July or early August. However, by this time the effects of a weakening easterly jet (Fig. 14) and increasing tidal amplitudes (Fig. 9) will combine to limit growth of the slower [0.5,3] mode. Fully interactive GCM simulations are needed to test this hypothesis by studying

the origin and growth of these various unstable modes in concert with fluctuations in the strength and curvature of the easterly jet for realistic conditions.

6. Summary and Discussion

Global synoptic meteorological analyses of the MLT from the NOGAPS-ALPHA data assimilation system have provided, for the first time, a comprehensive description of Q2DW behavior during the NH summers of 2007, 2008, and 2009. Unlike the SH case, where the Q2DW is primarily a westward propagating zonal wavenumber 3 feature, we find that the Q2DW in NH summer is comprised primarily of westward propagating zonal wavenumber 3 and wavenumber 4 components that are comparable in magnitude, consistent with earlier observational studies. Wavenumber 3 tends to maximize during July, while wavenumber 4 tends to maximize in late June and early August. We did not find evidence for significant Q2DW activity in the NH extratropics outside of the June–August period. At latitudes between 30° – 50°N, where the Q2DW amplitudes are largest, the wavenumber 3 and wavenumber 4 components are often anti-correlated throughout the NH summer season. Of the three summer periods examined here, the monthly mean wavenumber 3 Q2DW amplitudes are largest in July 2009 and smallest in July 2007, whereas the monthly mean amplitudes of the diurnal migrating tide at 30°N are largest in July 2007 and smallest in 2009.

Diagnostic calculations based on NOGAPS-ALPHA output indicate that the Q2DW originates from baroclinically unstable regions on the equatorward flank of the summer easterly jet near the 0.1 hPa level (∼65–70 km). The vertical propagation of the Q2DW activity appears to be controlled by the location of the critical line. The large wavenumber 3 amplitudes observed during July 2009 coincide with a relatively strong and well-defined

easterly jet core that directed more wave activity upward compared to July 2007, when the jet core was smaller and weaker.

Results from a linearized instability model using daily NOGAPS-ALPHA winds for summer 2009 as input show that the baroclinically unstable region near the summer easterly jet supports growth of both zonal wavenumber 3 and 4 disturbances with periods near 2 days. The growth times of these disturbances are typically in the range of 10–20 days during July, but approach ∼5 days in early August. Using a similar modeling approach based on winds from a mechanistic global circulation model (GCM), Rojas and Norton [2007] found evidence for two zonal wavenumber 3 modes with growth times between 3–5 days: a faster growing mode with period of 35 hours and a slower growing mode with a period of 42 hours. In this study, the faster growing mode quickly reached saturation at relatively small amplitude while the slower growing mode continued to grow to much larger amplitude and then began to interact with the background flow. In the present study, qualitatively similar behavior can be seen in the anti-correlation between the faster growing [0.5,4] and slower growing [0.5,3] components of the Q2DW (e.g., Fig. 10). We plan to pursue this subject further by conducting free-running model simulations using the NOGAPS-ALPHA meteorological fields as initial conditions to determine whether the [0.5,3] component interacts with the [0.5,4] components as it grows, or if the two components grow independently from one other.

Although the results of the 2DFFT analysis suggest an anticorrelation between the monthly mean amplitudes of the Q2DW and diurnal migrating tide during July, we do not find direct evidence for the type of interaction that can sometimes lead to rapid amplification of the Q2DW in SH summer [e.g. Norton and Thuburn, 1999; Palo et al.,

1999; McCormack et al., 2010; Hecht et al., 2010; Chang et al., 2011; Yue et al., 2012]. This is likely due to the smaller amplitudes and more broad band nature of the Q2DW in NH summer compared to SH summer, which reduces the chances for the type of interaction described by Walterscheid and Vincent [1996]. A modeling study of the SH Q2DW in January by Chang et al. [2011] found that nonlinear advection of momentum by the Q2DW itself may introduce variations in the background flow and, by extension, in tidal amplitudes that can also account for anti-correlation between the Q2DW and migrating diurnal tide. Other factors controlling the year-to-year variations in the strength and location of the NH summer easterly jet such as gravity wave activity may also play a role in controlling the behavior of both the Q2DW and tides. While the Q2DW-tide relationship in the SH summer has been the subject of numerous studies, there has been relatively little study of this relationship in the NH summer. To further investigate the nature of possible Q2DW-tidal coupling in NH summer, a targeted series of global circulation model (GCM) experiments capable of accurately simulating the evolution of the background zonal flow throughout the NH summer MLT is needed. Recently, Sassi et al. (*submitted*, 2013) used a GCM driven by NOGAPS-ALPHA meteorological fields in the lower atmosphere to generate a Q2DW in the the SH summer MLT internally through baroclinic instability processes, rather than through means of an imposed forcing. This approach will be extended to the NH summer cases of 2007, 2008, and 2009 in order to further investigate the nature of the Q2DW-tidal relationships presented here.

Acknowledgments. This work was supported in part by the Office of Naval Research and by the NASA Heliophysics Guest Investigator Program under award NNH09AK64I.

References

Andrews, D. G., J. R. Holton and C. B. Leovy (1987), *Middle Atmosphere Dynamics*, Academic Press, 489 pp.

Chou, M.-D. and Suarez, M. J. (2002): A solar radiation parameterization for atmospheric studies, NASA Tech. Mem. 10460, 15, *Technical Report Series on Global Modeling and Data Assimilation*, edited by Suarez, M. J., 52pp.

Chou, M.-D., Suarez, M. J., Liang, X. Z., and Yan, M.-H. (2001), A thermal infrared radiation parameterization for atmospheric studies, NASA Tech. Mem. 104606, 19, *Technical Report Series on Global Modeling and Data Assimilation*, edited by Suarez, M. J., 65pp.

Chang, L. C., S. E. Palo, and H.-L. Liu (2011), Short-term variability in the migrating diurnal tide caused by interactions with the quasi 2 day wave, *J. Geophys. Res., 116*, D12112, doi:10.1029/2010JD014996.

Coy, L. S. D. Eckermann, and F. Sassi (2011), Mesospheric precursors to the major stratospheric sudden warming of 2009: Validation and dynamical attribution using a ground-to-edge-of-space data assimilation system, *J. Adv. Model Earth Sys., 3*, doi:10.1029/2011/MS000067.

Daley, R. and E. Barker (2001), NAVDAS: Formulation and diagnostics, *Mon. Wea. Rev., 129*, 869–883.

Eckermann, S. D., K. W, Hoppel, L. Coy,, J. P. McCormack, D. E. Siskind, K. Nielsen, A. Kochenash, M. H. Stevens, and C. R. Englert (2009), High-altitude data assimilation system experiments for the Northern Hemisphere summer mesosphere season of 2007, *J. Atmos. Sol. Terr. Phys., 71*, doi:10.1016/j.jastp.2008.09.036.

736 Eckermann, S. D. (2009), Hybrid $\sigma - p$ coordinate choices for a global model, *Mon. Wea.*
737 *Rev., 137*, 224–245.

738 Eckermann, S. D. (2011), Explicitly stochastic parameterization of nonorographic gravity-
739 wave drag , *J. Atmos. Sci., 68*, 1749–1765.

740 Garcia, R. R., R. Lieberman, R., J. M. Russell, M. G. Mylnczak (2005), Large-scale
741 waves in the mesosphere and lower thermosphere observed by SABER, *J. Atmo. Sci.,*
742 *62*, 4384–4399.

743 Harris, T. J.: A long-term study of the quasi-two-day wave in the middle atmosphere, *J.*
744 *Atmos. Terr. Phys., 56*, 569–579.

745 Hartmann, D. L. (1983), Barotropic instability of the polar night jet, *J. Atmos. Sci., 40*,
746 817–835.

747 Hecht, J. H., R. L. Walterscheid, L. J. Gelinas, R. A. Vincent, I. M. Reid, and J. M.
748 Woithe (2010), Observations of the phase-locked 2 day wave over the Australian sec-
749 tor using medium-frequency radar and airglow data, *J. Geophys. Res., 115,* D16115,
750 doi:10.1029/2009JD013772.

751 Hayashi, Y. (1971), A generalized method of resolving disturbances into progressive and
752 retrogressive waves by space Fourier and time cross-spectral analyses, *J. Meteorol. Soc.*
753 *Japan, 49*, 125–128.

754 Hogan, T. and Rosmond, T. (1991), The description of the Navy Operational Global
755 Atmospheric Prediction System's spectral forecast model, Mon. Wea. Rev., 119, 1186–
756 1815, 1991.

757 Hoppel, K. W., N. L. Baker, L. Coy, S. D. Eckermann, J. P. McCormack, G. E. Nedoluha,
758 and D. E. Siskind (2008), Assimilation of stratospheric and mesospheric temperatures

759 from MLS and SABER into a global NWP model, *Atmos. Chem. Phys., 8*, 6103-6116.

760 Lieberman, R. S. (1999), Eliassen-Palm fluxes of the 2-day wave, *J. Atmo. Sci., 56*, 2846–

761 2861.

762 Lima, L. M., P. P. Batista, H. Takahashi,and B. R. Clemesha (2004), Quasi-

763 two-day wave observed by meteor radar at 22.7°S, *J. Atmos. Terr. Phys., 66*,

764 doi:10.1016/j.jastp.2004.01.007.

765 Limpasuvan, V., C. B. Leovy, and Y. J. Orsolini (2000), Observed temperature two-day

766 wave and its relatives near the stratopause, *J. Atmos. Sci., 57*, 1689–1701.

767 Limpasuvan, V., and D. L. Wu (2003), Two-day wave observations of UARS Microwave

768 Limb Sounder mesospheric water vapor and temperature, *J. Geophys. Res., 108* (D10),

769 4307, doi:10.1029/2002JD002903.

770 Limpasuvan, V. and D. L. Wu (2009), Anomalous two-day wave behavior during the 2006

771 austral summer, *Geophys. Res. Lett., 36,* L04807, doi:10.1029/2008GL036387.

772 Manney, G. L., and W. J. Randel (1993), Instability at the winter stratopause: A mech-

773 anism for the 4-day wave, *J. Atmos. Sci., 50*, 3928–3938.

774 McCormack, J. P., S. D. Eckermann, D. E. Siskind, and T. J. McGee (2006), CHEM2D-

775 OPP: A new linearized gas-phase ozone photochemistry parameterization for high-

776 altitude NWP and climate models, *Atmos. Chem. Phys., 6*, 4943-4972.

777 McCormack, J. P., K. W. Hoppel, and D. E. Siskind (2008), Parameterization of middle

778 atmospheric water vapor photochemistry for high-altitude NWP and data assimilation,

779 Atmos. Chem. Phys., 8, 7519-7532.

780 McCormack, J. P., L. Coy, and K. W. Hoppel (2009), Evolution of the quasi-two day wave

781 during January 2006, *J. Geophys. Res., 114*, D20, doi:10.1029/2009JD012239.

McCormack, J. P., S. D. Eckermann, K. W. Hoppel, and R. A. Vincent (2010), Amplification of the quasi-two day wave through nonlinear interaction with the migrating diurnal tide, *Geophys. Res. Lett., 37*, L16810, doi:10.1029/2010GL043906.

Muller, H. G., and L. Nelson (1978), A traveling quasi 2-day wave in the meteor region, *J. Atmos. Terr. Phys., 40*, 761-766.

Norton, W. A., and J. Thuburn (1999), Sensitivity of mesospheric mean flow, planetary waves, and tides to strength of gravity wave drag, *J. Geophys. Res., 104*, D24, 30,897–30,911.

Offermann, D., P. Hoffmann, P. Knieling, R. Koppmann, J. Oberheide, D. M. Riggin, V. M. Tunbridge, and W. Steinbrecht (2011), Quasi 2 day waves in the summer mesosphere: Triple structure of amplitudes and long-term development, *J. Geophys. Res., 116*, D00P02, doi:10.1029/2010JD015051, [printed 117(D4), 2012].

Orsolini, Y. J., V. Limpasuvan, and C. B. Leovy (1997), The tropical stratopause response in the UKMO stratospheric analyses: Evidence for a 2-day wave and inertial circulations, *Q. J. Roy. Meteorol. Soc., 123*, 1707-1724.

Palmer, T. N., G. J. Shutts, and R. Swinbank (1986): Alleviation of a systematic westerly bias in general-circulation and numerical weather prediction models through an orographic gravity-wave drag parametrization, *Quart. J. Roy. Meteor. Soc., 112*, 1001–1039.

Palo, S. E., R. G. Roble, M. E. Hagan (1999), Middle atmosphere effects of the quasi-two-day wave determined from a general circulation model, *Earth Panets Space, 51*, 629–647.

804 Pancheva, D. V. (2006), Quasi-2-day wave and tidal variability observed over
805 Ascension Island during January/February 2003, *J. Atmos. Terr. Phys., 68*,
806 doi:10.1016/j.jastp.2005.02.028.

807 Pfister, L. (1985), Baroclinic instability of easaterly jets with applications to the summer
808 mesosphere, *J. Atmos. Sci., 42*, 313–330.

809 Plumb, R. A. (1983), Baroclinic instability of the summer mesosphere: A mechanism for
810 the quasi-two-day wave?, *J. Atmos. Sci., 40*, 262–270.

811 Randel, W. J. (1994), Observations of the 2-day wave in NMC stratospheric analyses, *J.*
812 *Atmos. Sci., 51*, 306–313.

813 Rojas, M. and W. Norton (2007), Amplification of the 2-day wave from mutual interaction
814 of the global Rossby-gravity and local modes in the summer mesosphere, *J. Geophys.*
815 *Res., 112*, D12114, doi:10.1029/2006JD008084.

816 Salby, M. L. (1981), The 2-day wave in the middle atmosphere: Observations and theory,
817 *J. Geophys. Res., 86*, C10, 9654–9660.

818 Salby, M., and P. Callaghan (2000), Seasonal amplification of the 2-day wave: Relationship
819 between normal mode and instability, *J. Atmos. Sci., 58*, 1858–1869

820 Salby, M. L., and P. F. Callaghan (2008), Interaction of the 2-day wave with solar tides,
821 *J. Geophys. Res., 113*, D14121, doi:10.1029/2006JD007892.

822 Stevens, M. H., D. E. Siskind, S. D. Eckermann, L. Coy, J. P. McCormack, C. R. Englert,
823 K. W. Hoppel, K. Nielsen, A. J. Kochenash, M. E. Hervig, C. E. Randall, J. Lumpe,
824 S. M. Bailey, M. Rapp, P. Hoffmann, and J. Fiedler (2010), Tidally induced variations
825 of PMC altitudes and ice water content using a data assimilation system, *J. Geophys.*
826 *Res., 115*, D18209, doi:10.1029/2009JD013225.

827 Suresh Babu, V., K. Kishore Kumar, S. R. John, K. V. Subrahmanyam, and G.
828 Ramkumar (2011), Meteor radar observations of short-term variability of quasi 2 day
829 waves and their interaction with tides and planetary waves in the mesospherelower
830 thermosphere region over Thumba (8.5N, 77E), *J. Geophys. Res., 116*, D16121,
831 doi:10.1029/2010JD015390.

832 Teitelbaum, H. and F. Vial (1991), On tidal variability induced by nonlinear interaction
833 with planetary waves, *J. Geophys. Res., 96*, A8, doi:10.1029/91JA01019, 14,169–14,178.

834 Tunbridge, V. M., D. J. Sandford, and N. J. Mitchell (2011), Zonal wave numbers of the
835 summertime 2 day planetary wave observed in the mesosphere by EOS Aura Microwave
836 Limb Sounder, *J. Geophys. Res., 116*, D11103, doi:10.1029/2010JD014567.

837 Walterscheid, R. L., and R. A. Vincent (1996), Tidal generation of the phase-locked 2-day
838 wave in the southern hemisphere summer by wave-wave interactions, *J. Geophys. Res.,*
839 *101*, D21, doi:10.1029/96JD02248, 26,567–26,576.

840 Wu, D. L., P. B. Hays, R. W. Skinner, A. R. Marshall, M. D. Burrage, R. S. Lieber-
841 man, and D. A. Ortland (1993), Observations of the quasi 2-day wave from the High
842 Resolution Doppler Imager on UARS, *Geophys. Res. Lett., 20* (24), 2853–2856.

843 Wu, D. L., E. F. Fishbein, W. G. Read, and J. W. Waters (1996), Excitation and evolution
844 of the quasi-2-day wave observed in UARS/MLS temperature measurements, *J. Atmos.*
845 *Sci., 53*, 5, 728–738.

846 Wu, Q., D. A. Ortland, T. L. Killeen, R. G. Roble, M. E. Hagan, H.-L. Liu, S. C.
847 Solomon, J. Xu, W. R. Skinner, and R. J. Niciejewski (2008), Global distribution and
848 interannual variations of mesospheric and lower thermospheric neutral wind diurnal
849 tide: 1. Migrating tide, *J. Geophys. Res., 113*, doi:10.1029/2007JA012542.

Yue, J., H.-L. Liu, and L. C. Chang (2012), Numerical investigation of the quasi 2 day wave in the mesosphere and lower thermosphere, *J. Geophys. Res., 117*, D05111, doi:10.1029/2011JD016574.

Table 1. Correlation coefficients among [1,1], [0.5,3] and [0.5,4] meridional wind amplitudes at 30°N and 0.0036 hPa during July.

Year	[1,1] vs. [0.5,3]	[1,1] vs. [0.5,4]	[0.5,3] vs. 0.5,4]
2007	0.16	0.26	-0.47
2008	-0.35	-0.44	0.2
2009	0.00	0.1	-0.42

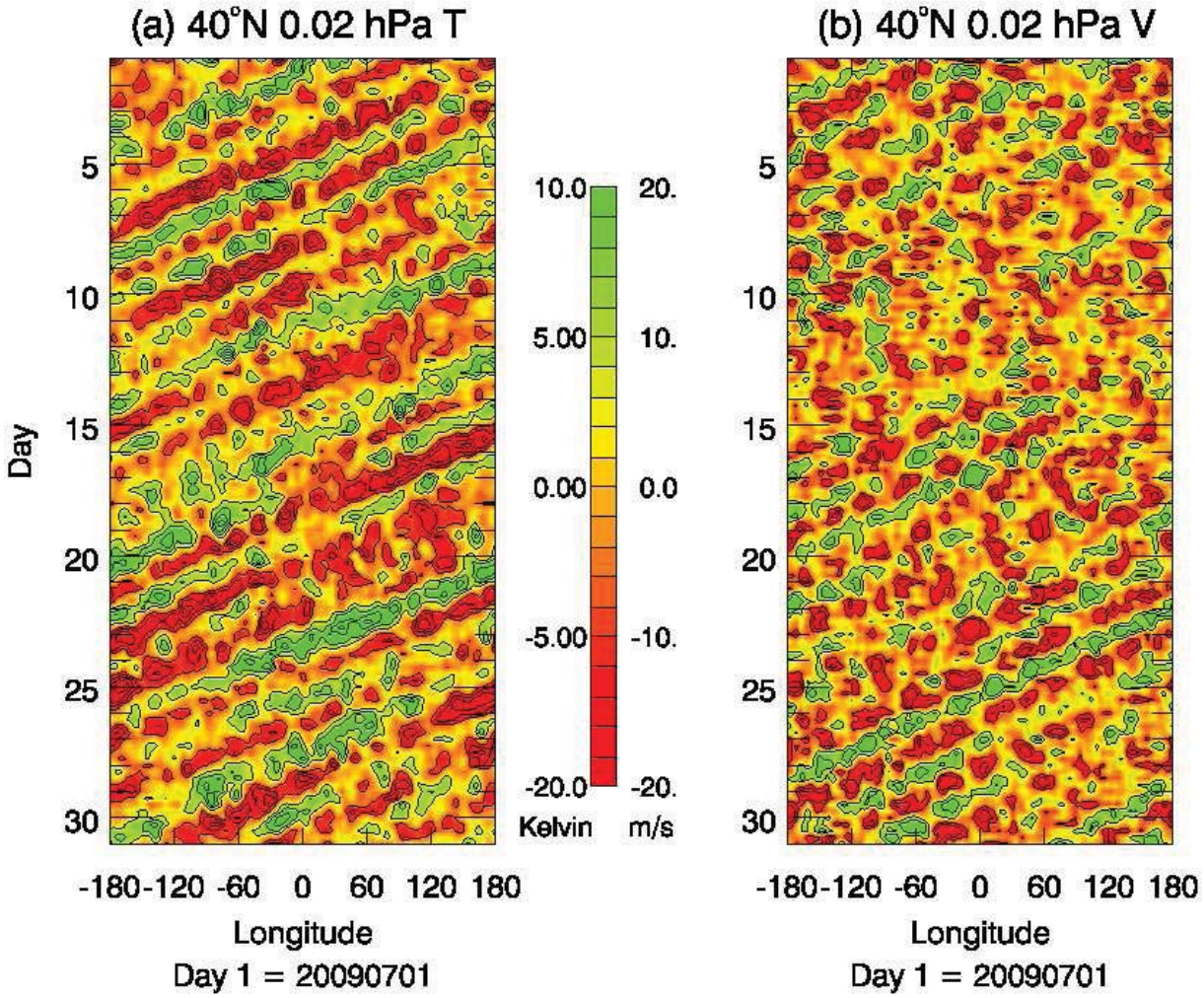

Figure 1. Hovmöller plot of NOGAPS-ALPHA (a) temperature and (b) meridional wind anomalies at 40°N and 0.02 hPa for July 2009.

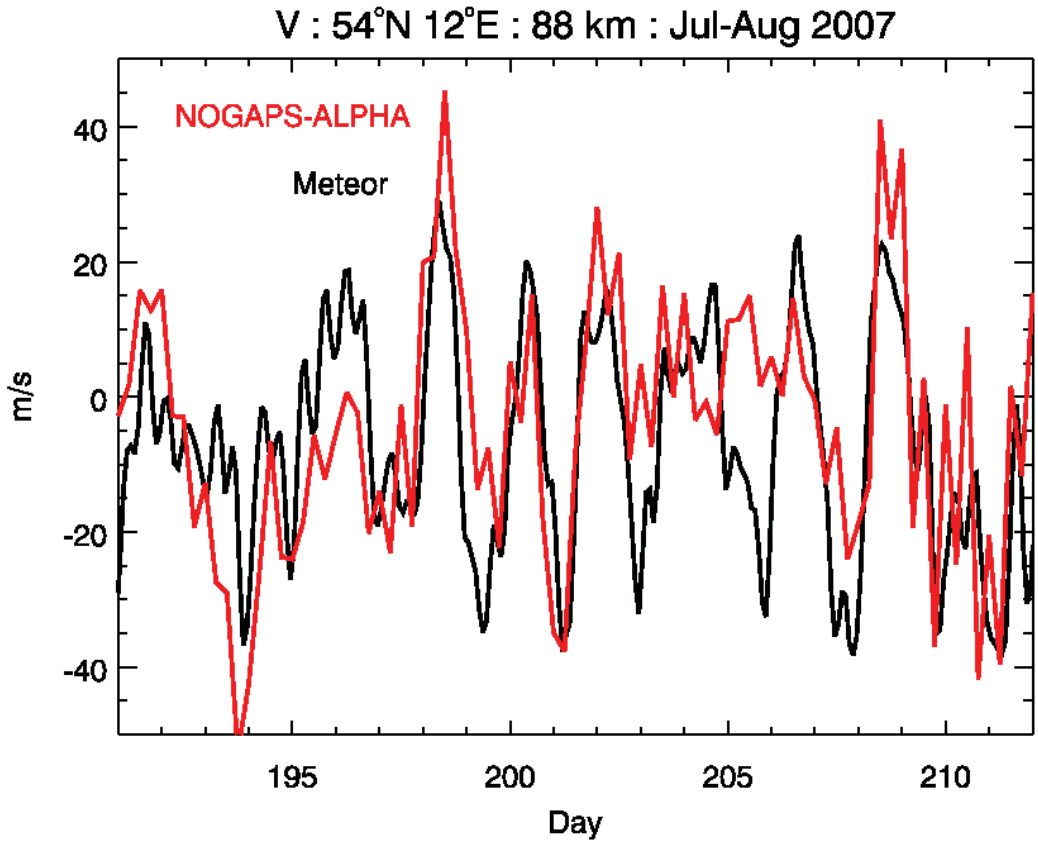

Figure 2. Time series of meridional winds from meteor radar observations over Kühlungsborn at 88 km (black curve) and from coincident NOGAPS-ALPHA analyses at 0.0036 hPa (red curve) during July – August 2007.

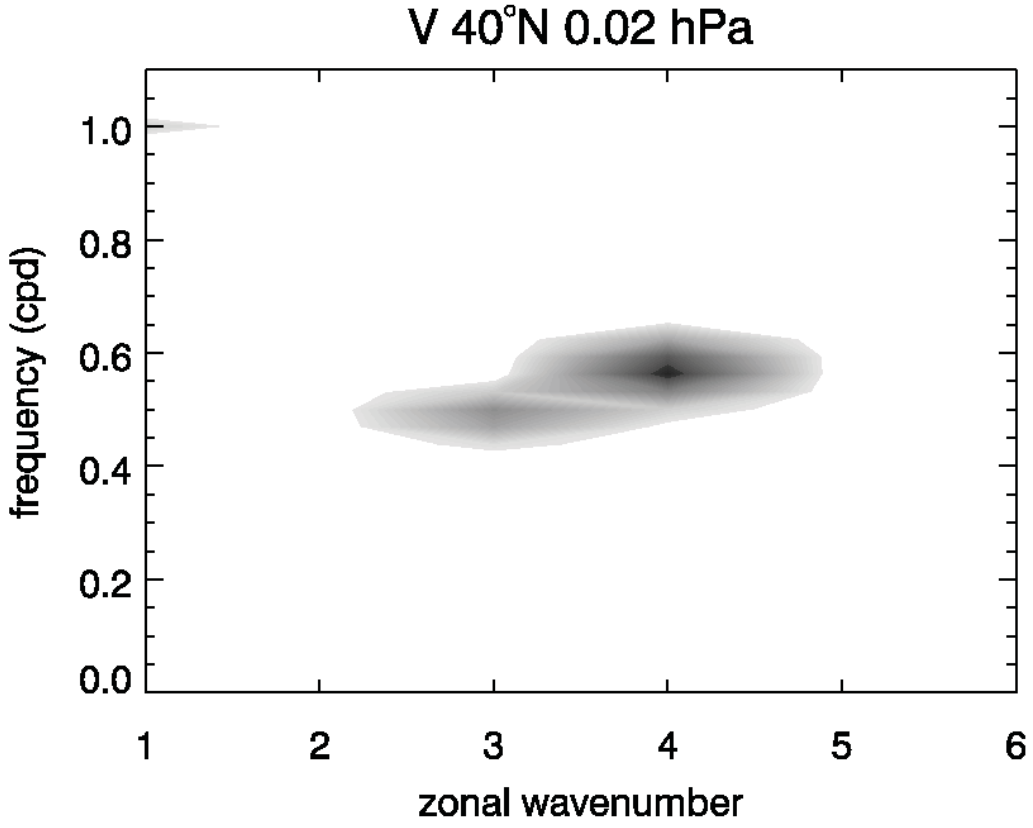

Figure 3. Normalized power spectrum obtained from 2DFFT of NOGAPS-ALPHA meridional winds at 40°N and 0.021 hPa. Positive frequencies denote westward propagation.

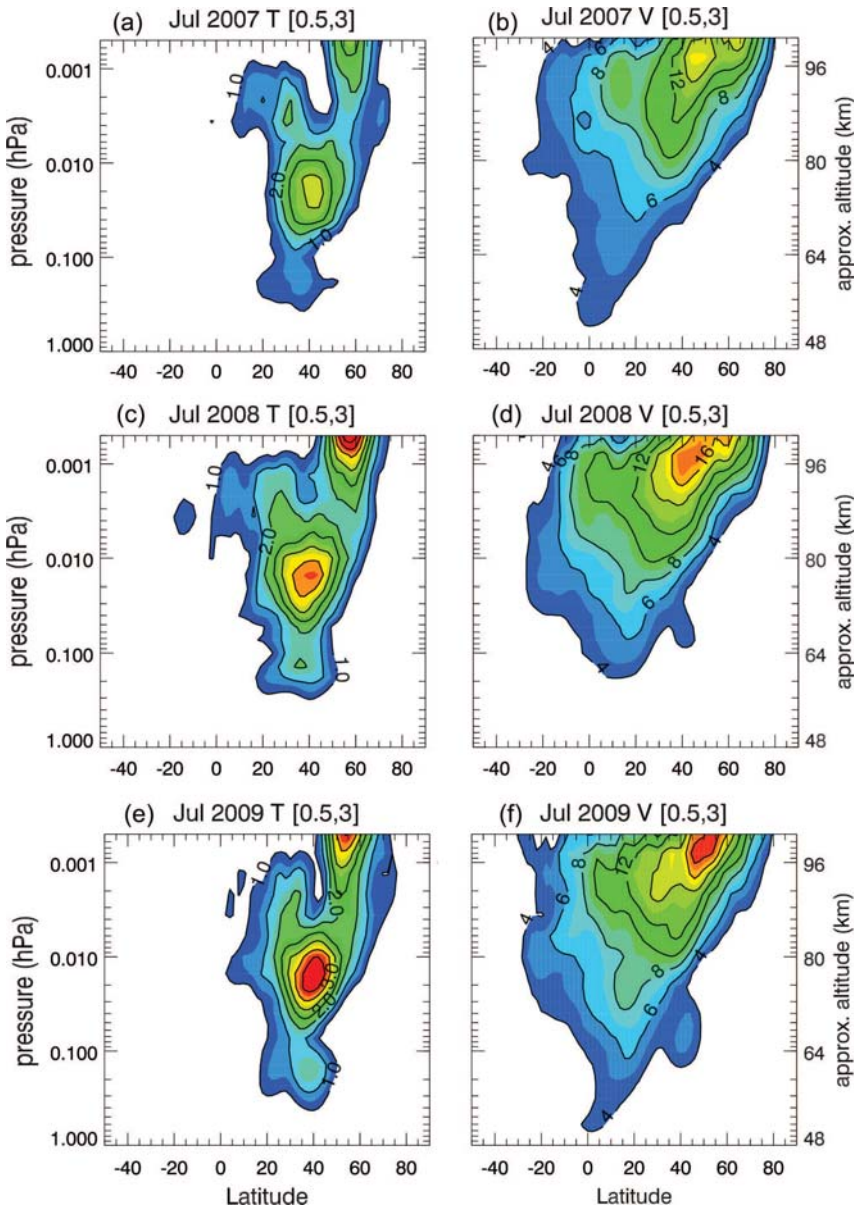

Figure 4. Monthly mean amplitudes of the [0.5,3] Q2DW component in temperature and meridional wind for July 2007, 2008, and 2009. Contour intervals are 0.5 K and 2 m s^{-1}.

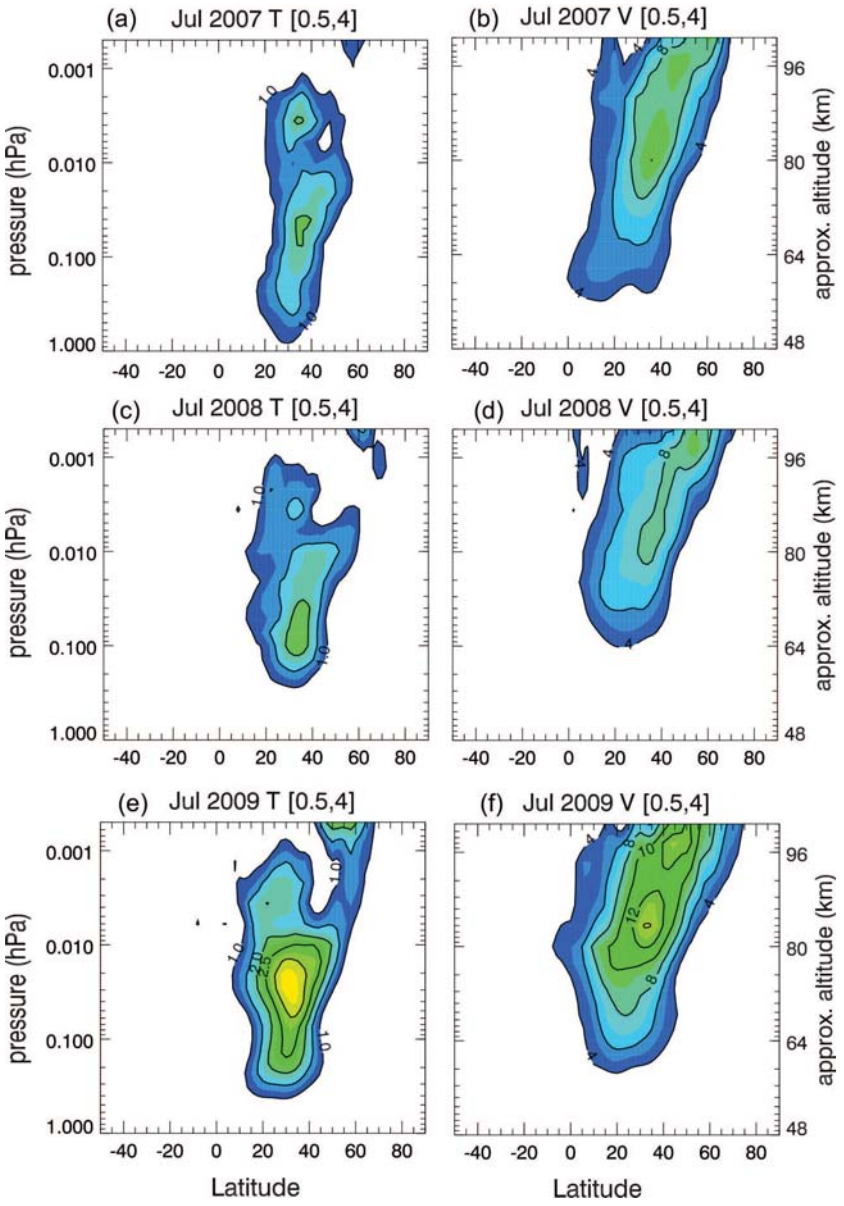

Figure 5. Monthly mean amplitudes of the [0.5,4] Q2DW component in temperature and meridional wind 1428 for July 2007, 2008, and 2009. Contour intervals are 0.5 K and 2 m s^{-1}.

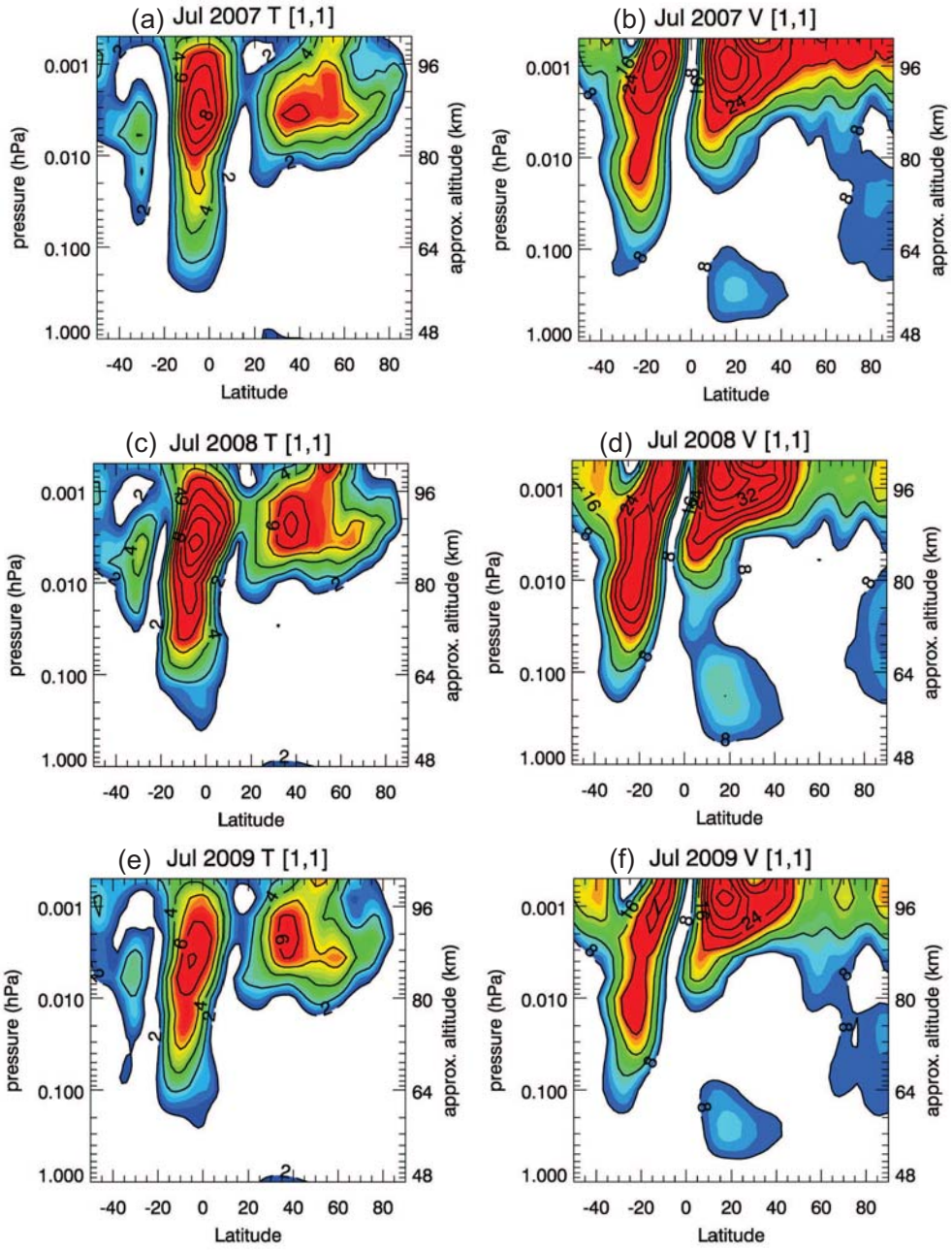

Figure 6. Monthly mean amplitudes of the [1,1] migrating diurnal tide in temperature and meridional wind 1428 for July 2007, 2008, and 2009. Contour intervals are 1 K and 4 m s^{-1}.

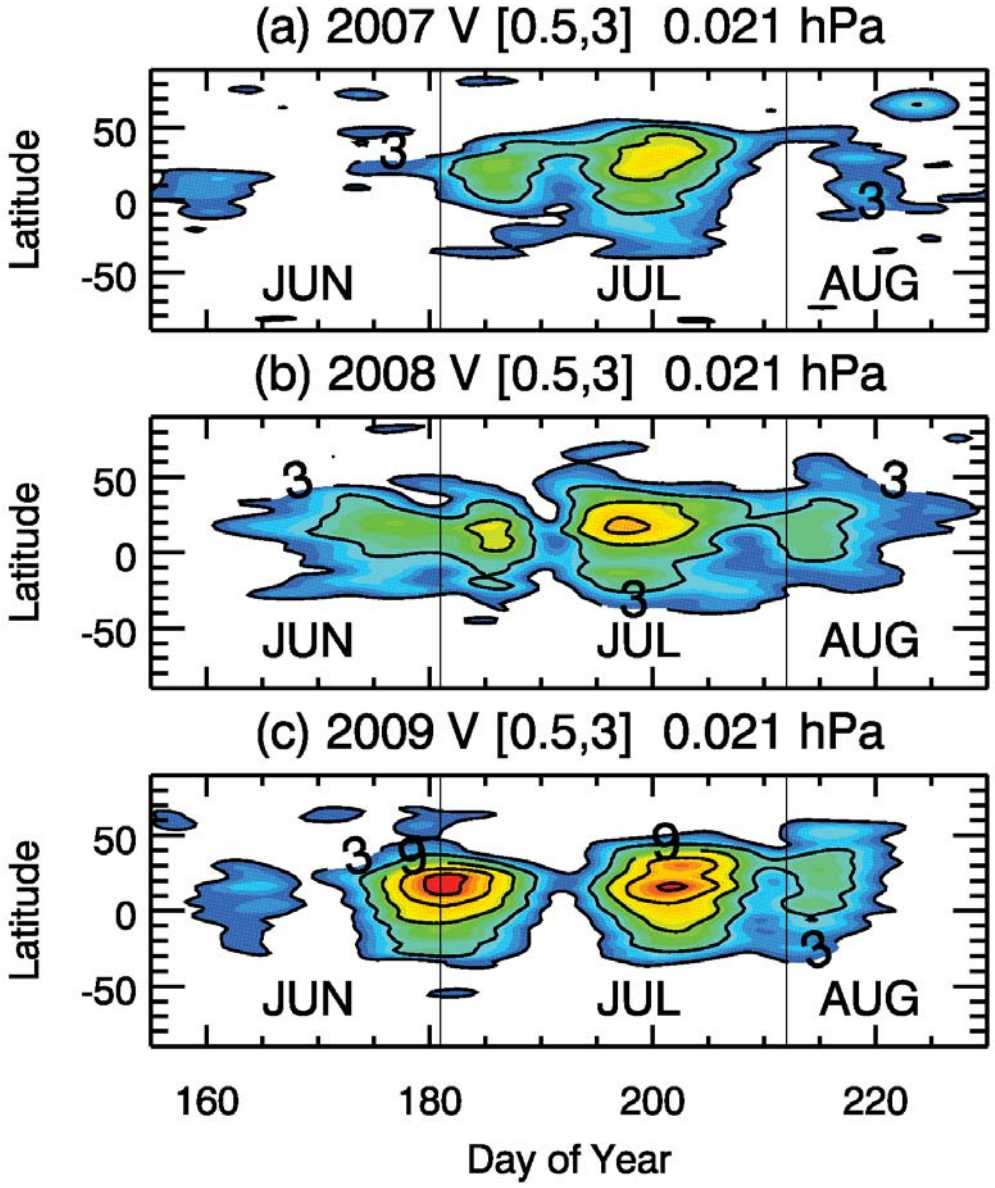

Figure 7. Latitude-time section of [0.5,3] Q2DW amplitudes at 0.021 hPa for the June–August period of (a) 2007, (b) 2008, and (c) 2009. Contour interval is 3 K.

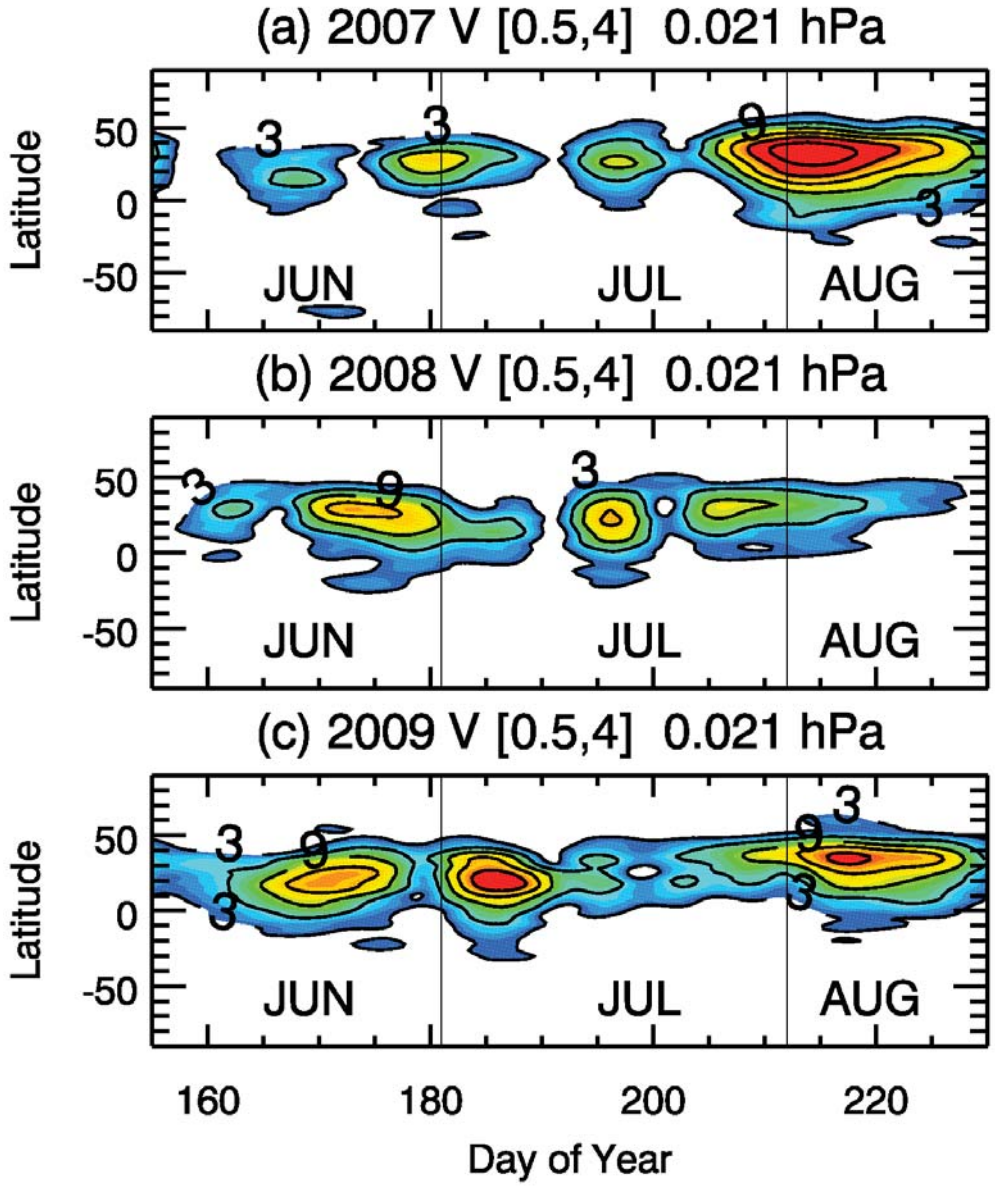

Figure 8. Latitude-time section of [0.5,4] Q2DW amplitudes at 0.021 hPa for the June–August period of (a) 2007, (b) 2008, and (c) 2009. Contour interval is 3 K.

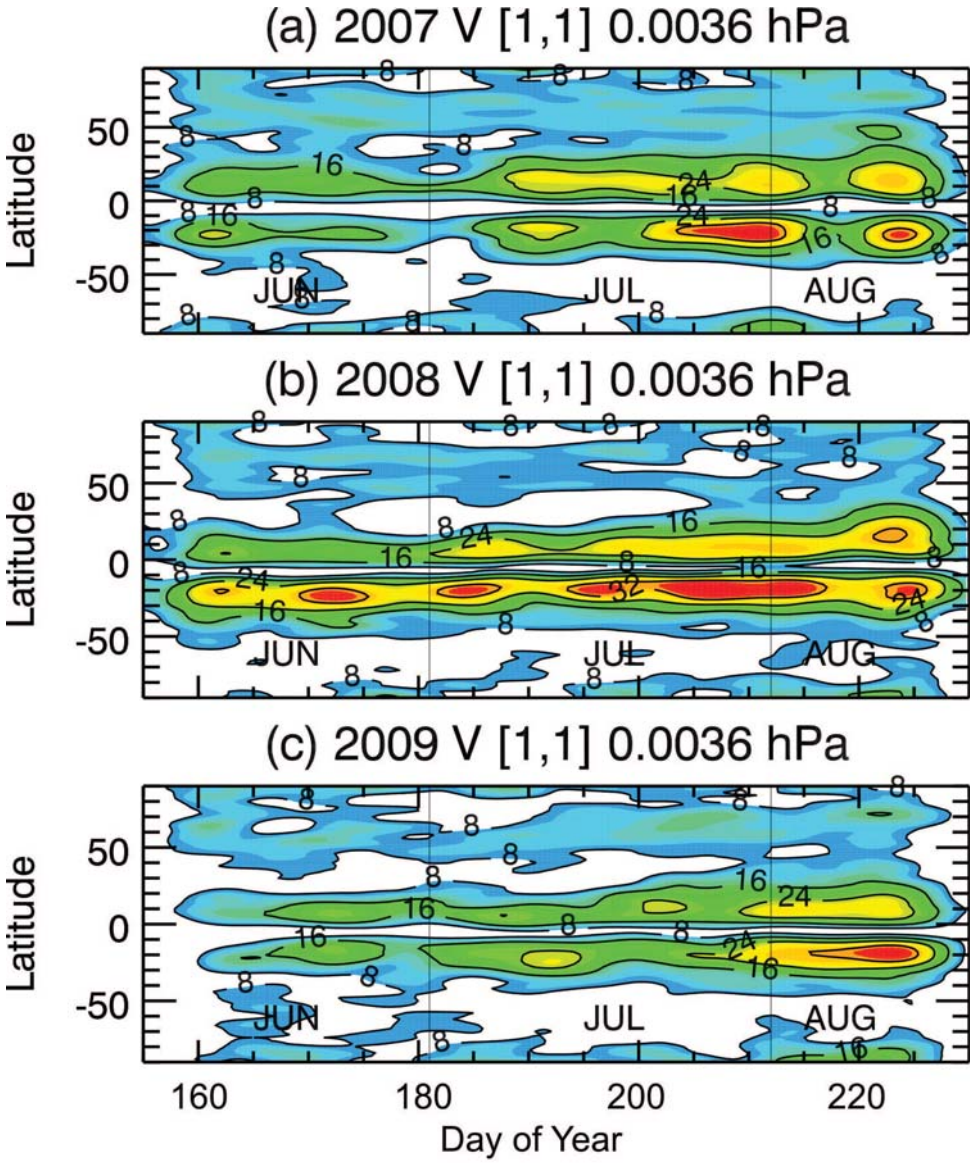

Figure 9. Latitude-time section of [1,1] tidal amplitudes at 0.0036 hPa for the June–August period of (a) 2007, (b) 2008, and (c) 2009. Contour interval is 8 m s^{-1}.

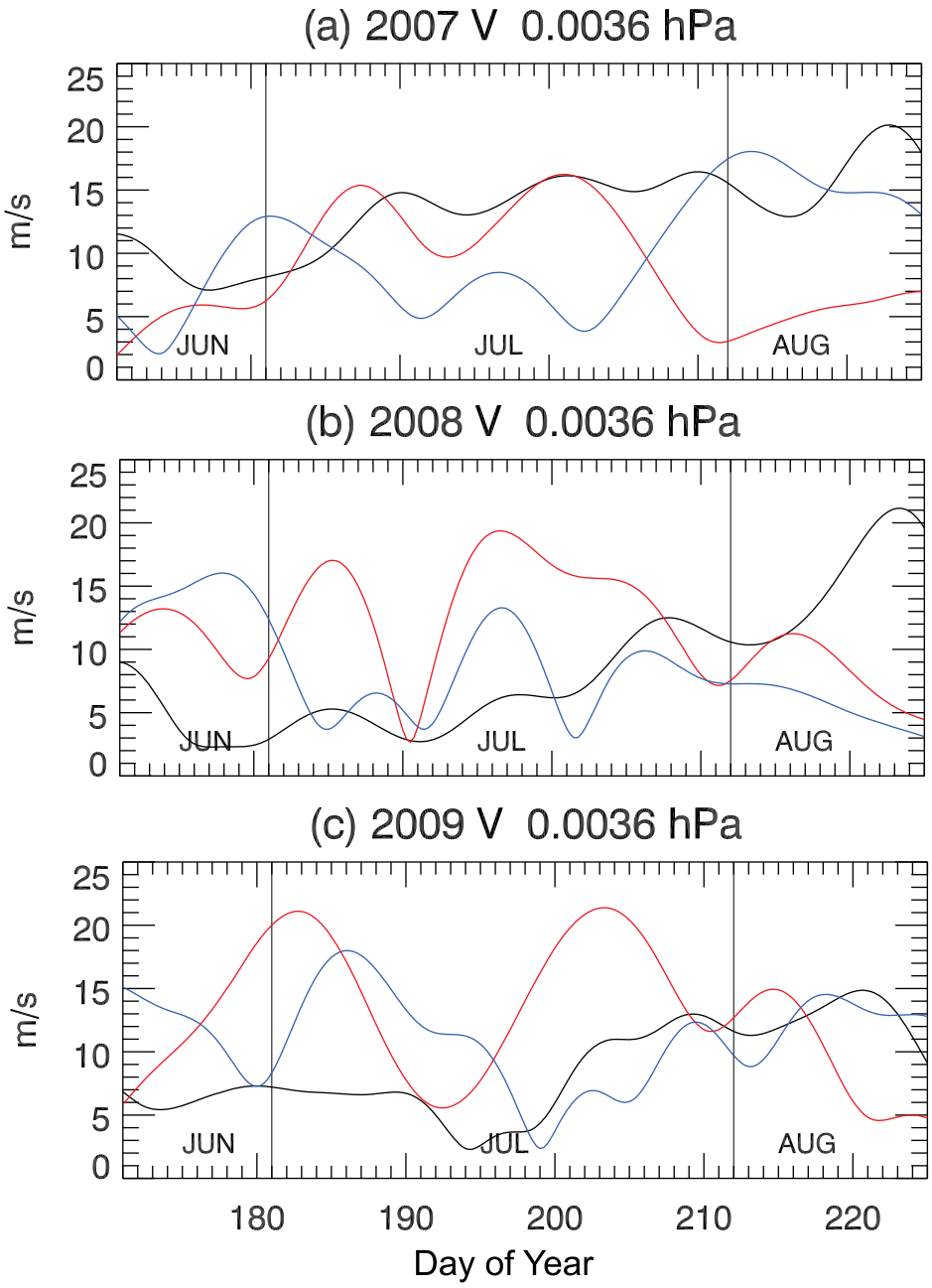

Figure 10. Time series of the [0.5,3] (red), [0.5,4] (blue), and [1,1] (black) amplitudes at 30°N and 0.0036 hPa during June–August of (a) 2007, (b) 2008, and (c) 2009.

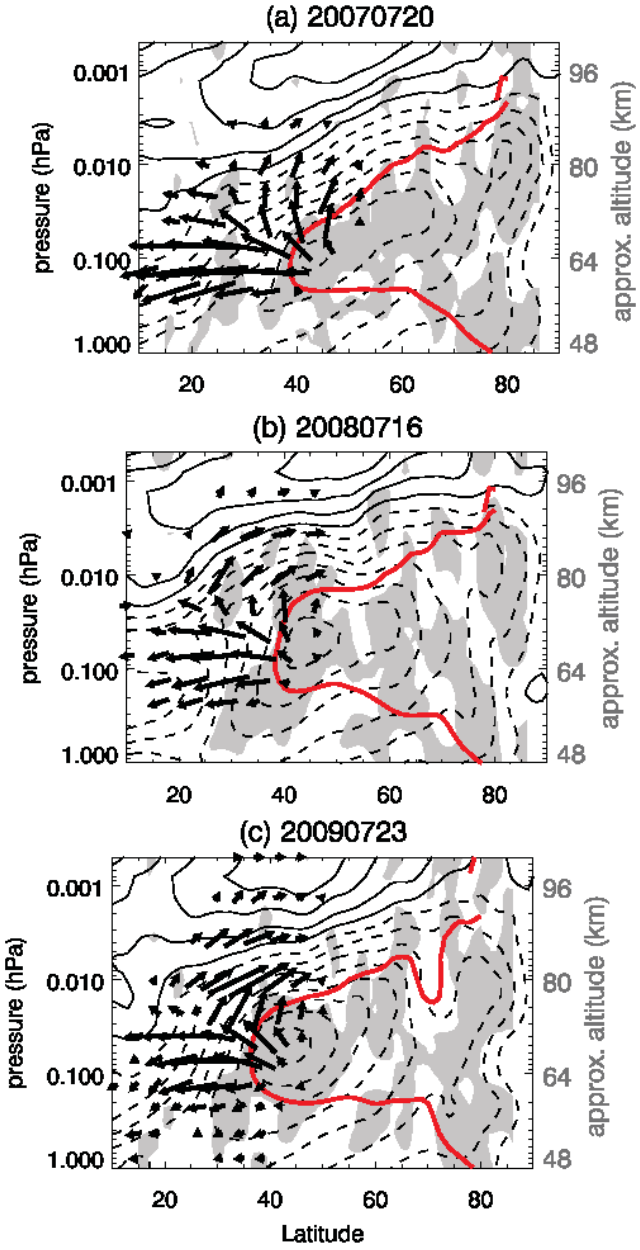

Figure 11. Contour plots of daily averaged NOGAPS-ALPHA zonal mean zonal winds for (a) July 20, 2007, (b) July 16, 2008, and (c) July 23, 2009. Contour interval is 10 m s^{-1}; dashed contours represent easterly winds. Shaded regions indicate where meridional gradient in quasi-geostrophic potential vorticity is negative. Red contour indicates approximate location of critical line for [0.5,3] Q2DW. Arrows represent EP-fluxes associated with the [0.5,3] Q2DW.

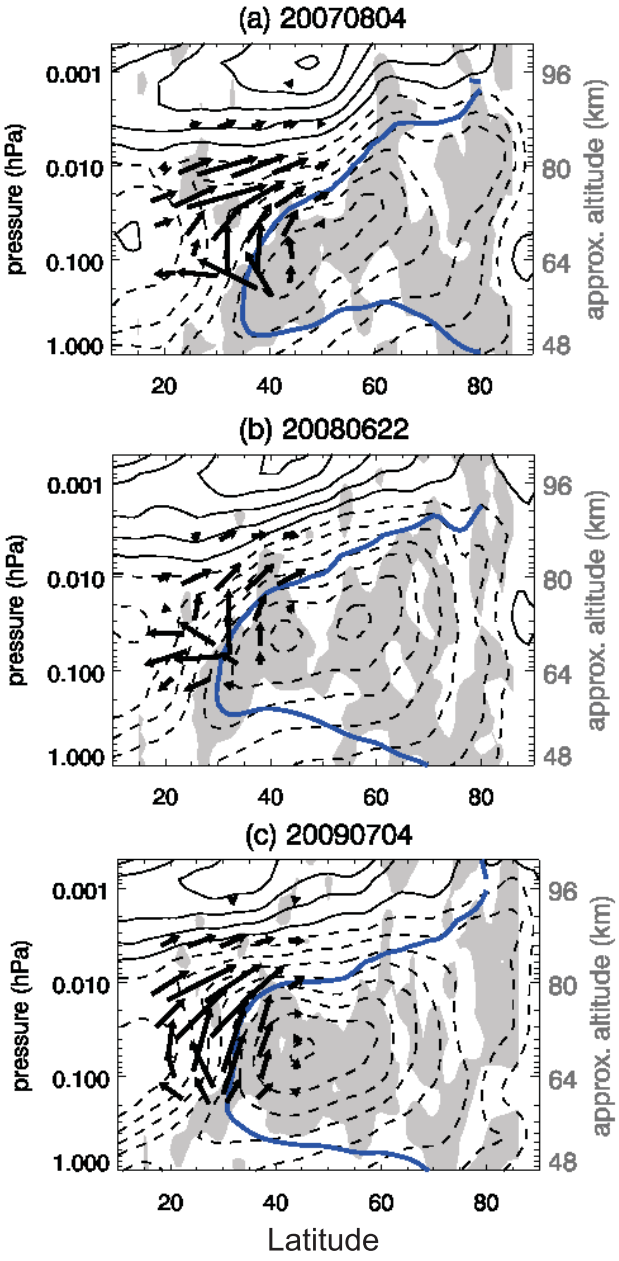

Figure 12. Contour plots of daily averaged NOGAPS-ALPHA zonal mean zonal winds for (a) August 4, 2007, (b) June 22, 2008, and (c) July 4, 2009, as in Fig. 11. Blue contour indicates approximate location of critical line for [0.5,4] Q2DW. Arrows represent EP-fluxes associated with the [0.5,4] Q2DW.

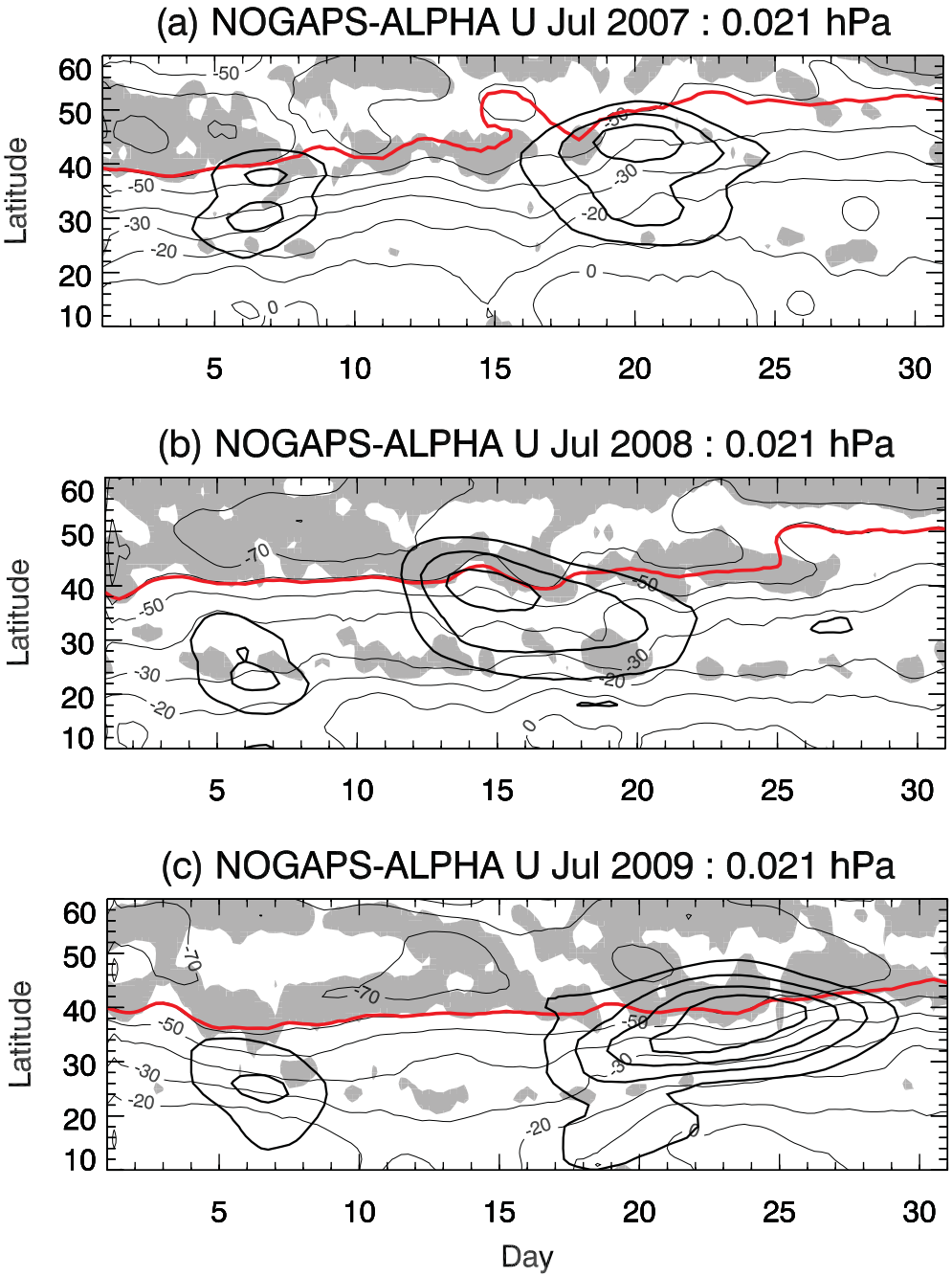

Figure 13. Latitude-time sections of daily averaged NOGAPS-ALPHA zonal mean zonal winds at 0.021 hPa during July of (a) 2007, (b) 2008, and (c) 2009. Shaded regions indicate where meridional gradient in quasi-geostrophic potential vorticity is negative. Red contour indicates approximate location of critical line for [0.5,3] Q2DW. Heavy black contours indicating positive [0.5,3] Q2DW eddy heat flux are drawn at values of 10, 15, 20, 25 K m s^{-1}

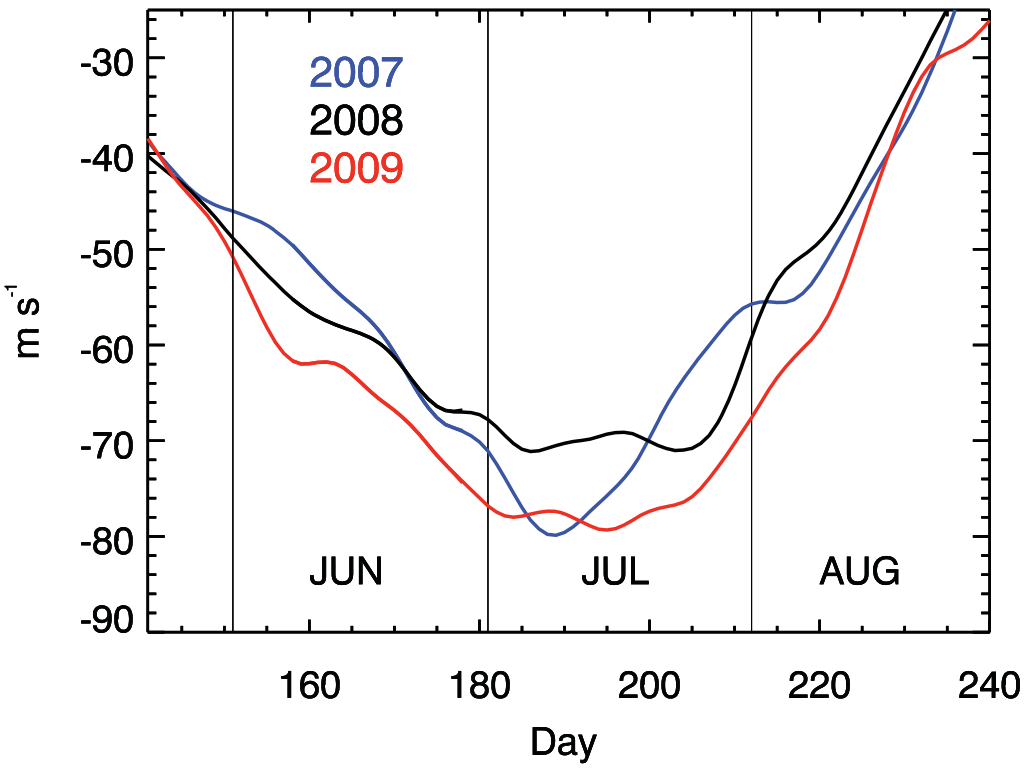

Figure 14. Time series of zonal mean zonal wind speed at 40°N and 0.1 hPa during NH summer of 2007 (blue curve), 2008 (black curve), and 2009 (red curve).

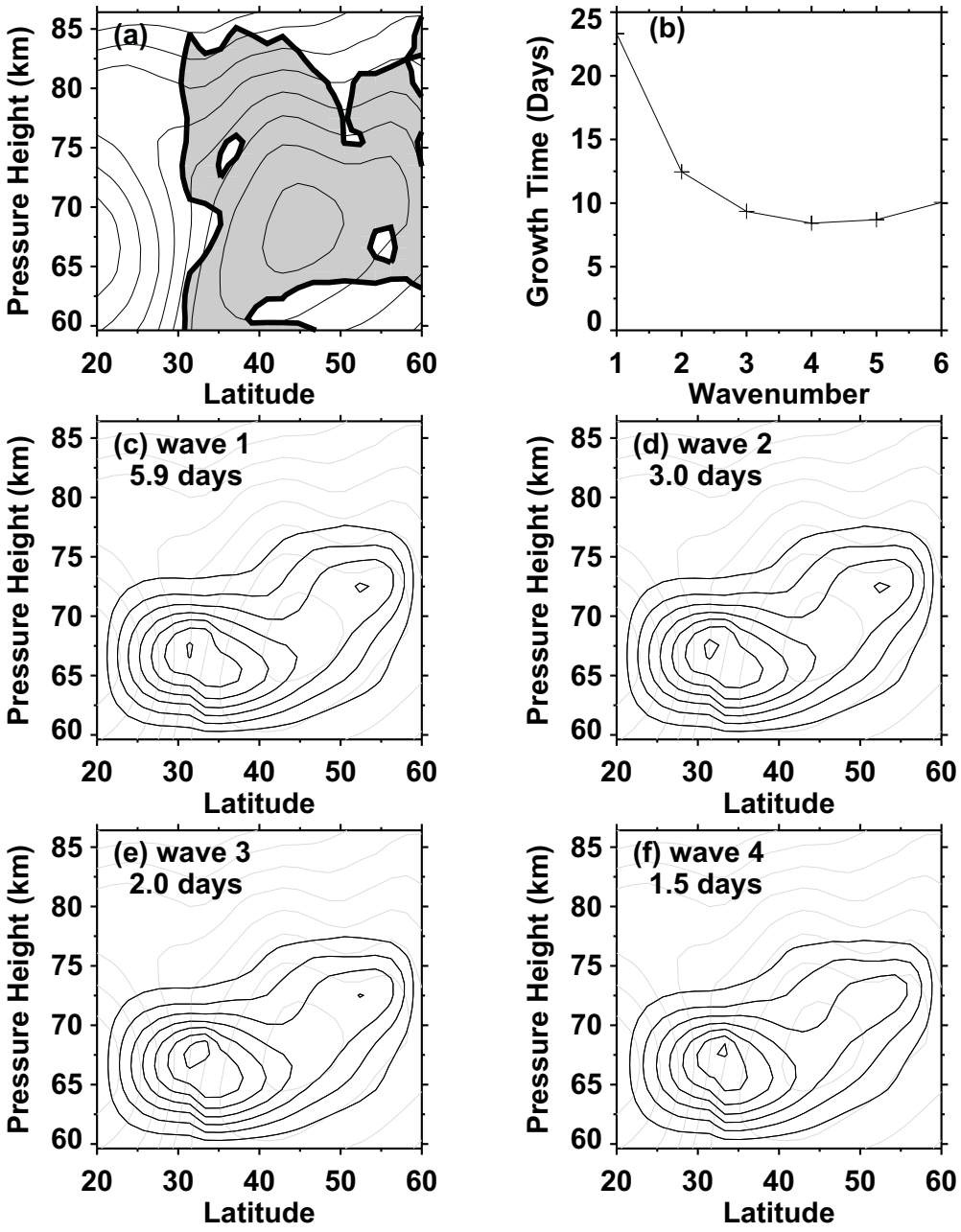

Figure 15. Linear instability model results for July 10, 2009 case. (a) Latitude-altitude distribution of zonal winds (contour interval of 10 m s^{-1}), shaded regions indicate where q_y ¡ 0; (b) e-folding times for westward-propagating unstable modes as function of zonal wavenumber; (c)-(f) normalized amplitudes of the geostropic streamfunction solutions, and the period of each solution, for wavenumbers 1 through 4 .

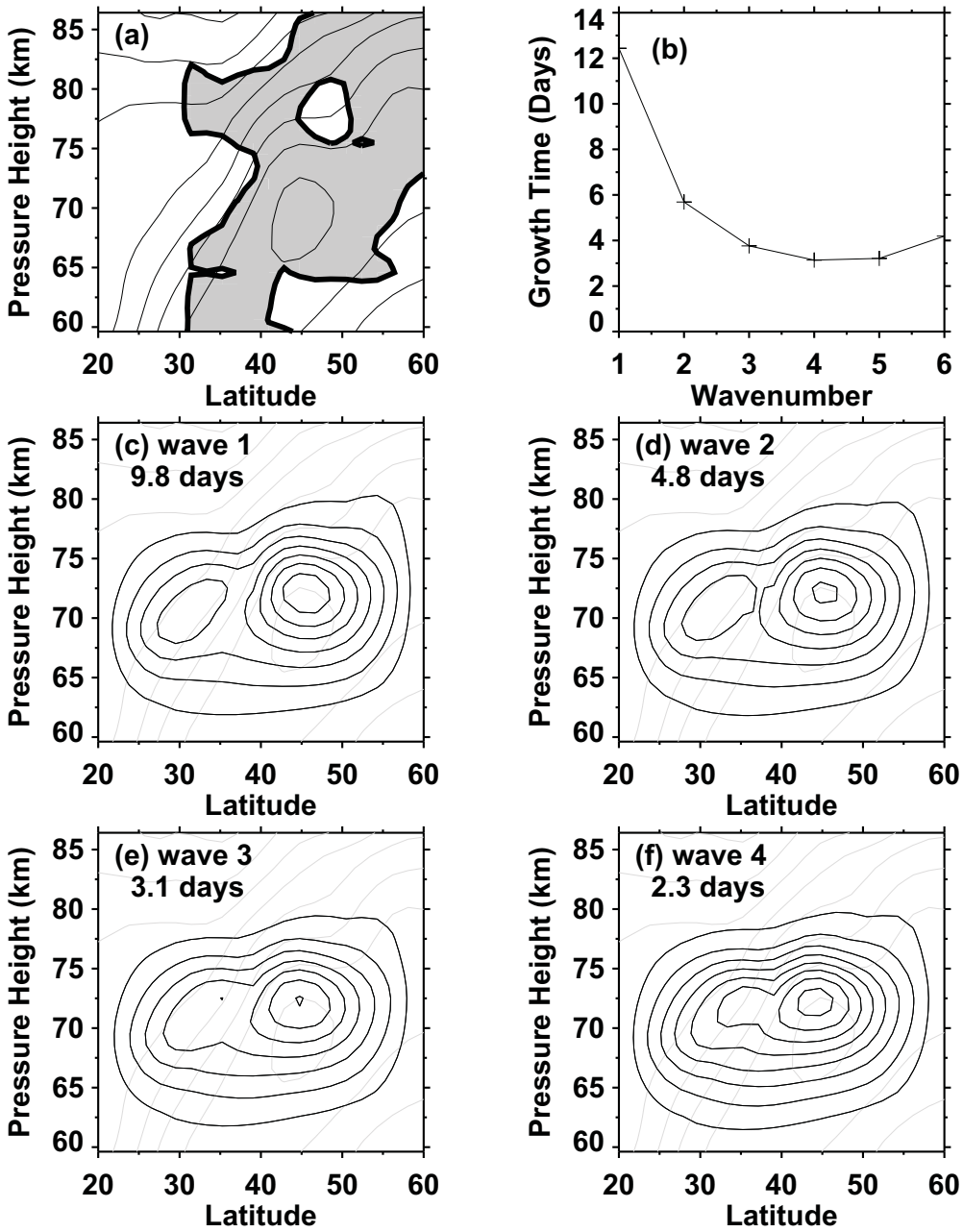

Figure 16. As in Figure 15, but for the August 5, 2099 case.

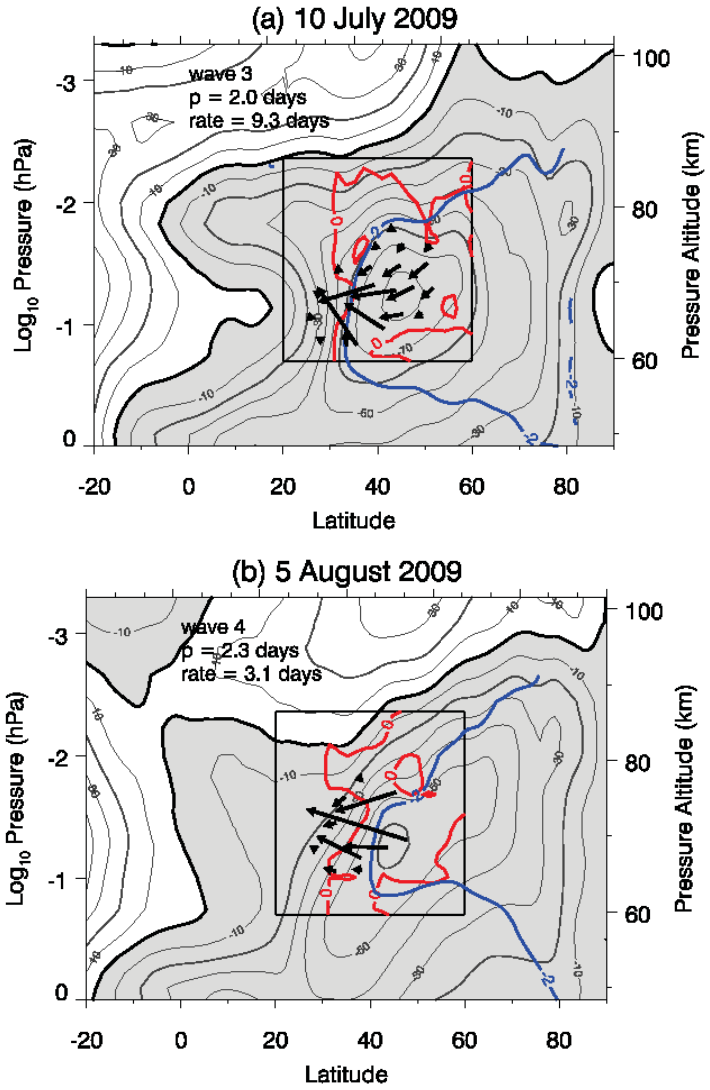

Figure 17. Daily averaged NOGAPS-ALPHA zonal mean zonal winds for (a) July 10 2009 and (b) August 5, 2009. Shaded regions indicate easterly flow. The domain of the linear instability model is indicated by the box extending from 20°–60°N and 60–86 km. Red contour encloses region where q_y ¡ 0, blue contour indicates approximate location of critical line for wave solution with period closest to 48 hours. Arrows represent EP-flux vectors derived from zonal wavenumber 3 and 4 solutions of the linear instability model

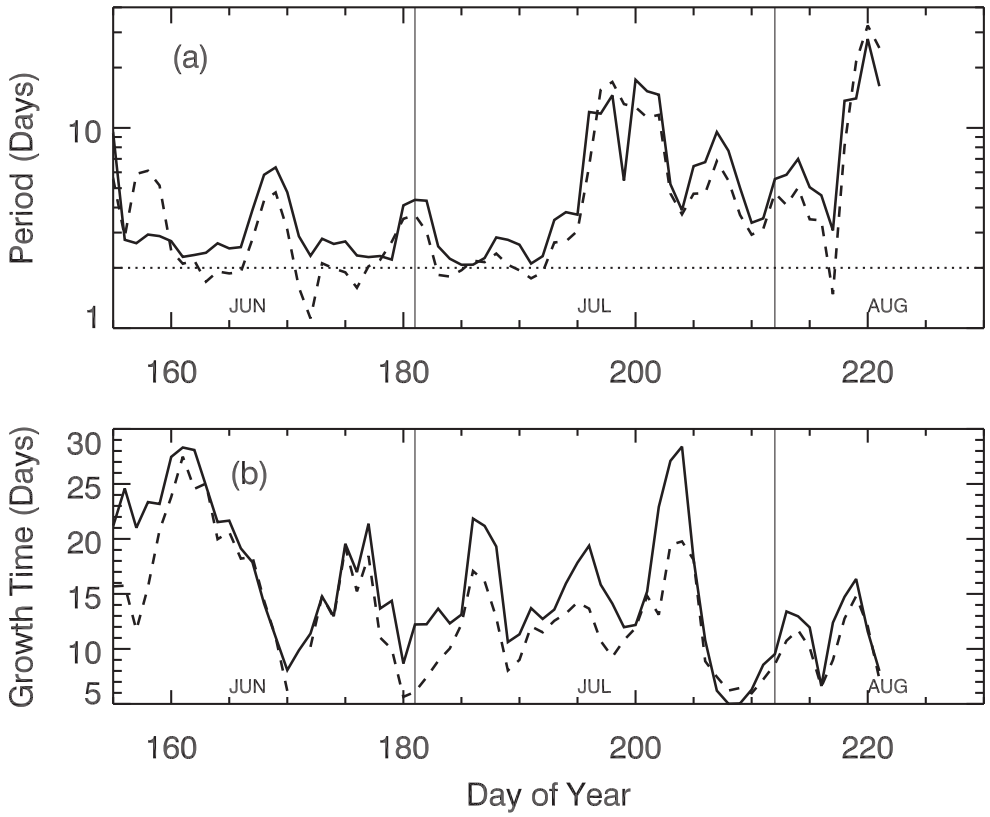

Figure 18. Time series of (a) period and (b) e-folding time for zonal wavenumber 3 (solid curve) and wavenumber 4 (dashed curve) instability model solutions during summer 2009. Dashed line drawn at 2 days.